scientific reports

Check for updates

OPEN

Leaf scale quantification of the effect of photosynthetic gas exchange on Δ_{47} of CO_2

Getachew Agmuas Adnew[1,6]✉, Magdalena E. G. Hofmann[1,5,6], Thijs L. Pons[2], Gerbrand Koren[3], Martin Ziegler[4], Lucas J. Lourens[4] & Thomas Röckmann[1]

The clumped isotope composition (Δ_{47}, the anomaly of the mass 47 isotopologue relative to the abundance expected from a random isotope distribution) of CO_2 has been suggested as an additional tracer for gross CO_2 fluxes. However, the effect of photosynthetic gas exchange on Δ_{47} has not been directly determined and two indirect/conceptual studies reported contradicting results. In this study, we quantify the effect of photosynthetic gas exchange on Δ_{47} of CO_2 using leaf cuvette experiments with one C_4 and two C_3 plants. The experimental results are supported by calculations with a leaf cuvette model. Our results demonstrate the important roles of the Δ_{47} value of CO_2 entering the leaf, kinetic fractionation as CO_2 diffuses into, and out of the leaf and CO_2–H_2O isotope exchange with leaf water. We experimentally confirm the previously suggested dependence of Δ_{47} of CO_2 in the air surrounding a leaf on the stomatal conductance and back-diffusion flux. Gas exchange can enrich or deplete the Δ_{47} of CO_2 depending on the Δ_{47} of CO_2 entering the leaf and the fraction of CO_2 exchanged with leaf water and diffused back to the atmosphere, but under typical ambient conditions, it will lead to a decrease in Δ_{47}.

The carbon dioxide (CO_2) concentration in the atmosphere is controlled by various large exchange fluxes with the bio-, hydro- and geosphere, and by anthropogenic emissions. Important tools for quantifying the different terms of the budget are measurement of the mole fraction and the isotopic composition of CO_2[1]. The stable carbon isotope composition allows to distinguish between the CO_2 uptake by the ocean and by plants[2], and the stable oxygen isotope composition allows to determine the magnitude of the large gross carbon fluxes between the atmosphere and biosphere[3–6]. Recent advancements in precise measurement techniques of ^{17}O-excess[7] enable the ^{17}O-excess, $\Delta^{17}O$, of tropospheric CO_2 to be used as tracer of terrestrial gross primary production[8–13] or stratospheric influx[14–16]. In addition, the analysis of radiocarbon has been used to quantify the amount of anthropogenic CO_2 emissions[17,18]. Despite these four independent isotopic tracers, the CO_2 budget still remains uncertain. It has been suggested that the abundance of the isotopologue $^{18}O^{13}C^{16}O$ in the atmosphere might be a promising new tracer to complement the existing isotope tracers[19–23].

The abundance of the double substituted (i.e., contain two rare isotopes) isotopologue $^{13}C^{18}O^{16}O$, compared to its abundance at stochastic isotope distribution for a given bulk composition, is also referred to as the clumped isotopic composition of CO_2 (Δ_{47}, see Sect. "Theory" for definition). One of the main reasons for its applicability as a tracer to constrain CO_2 fluxes is that it is mainly sensitive to the temperature at which the CO_2 is formed or exchanges isotopes with water[19]. A disadvantage of using Δ_{47} is that signals are very small: For typical ambient surface temperatures of 5 to 30 °C, the thermodynamic equilibrium value of Δ_{47} ranges between 0.90 to 1.04 ‰[19,24,25], so high precision measurements are required. Thermodynamic equilibrium values of Δ_{47} decrease towards 0 at increasingly higher temperatures, and it is possible to distinguish high temperature (e.g. combustion) from low temperature process (e.g. respiration) using Δ_{47}[19,20,22,26].

It is well established that oxygen isotope exchange between CO_2 and water in the biosphere and hydrosphere is the dominant process controlling the oxygen isotope composition of atmospheric CO_2[27,28]. The CO_2–H_2O exchange in soils and leaf water is catalyzed by the enzyme carbonic anhydrase (CA)[27,29–31]. In the leaf, CO_2–H_2O exchange takes place in the mesophyll, and the mole fraction of the CO_2 at the CO_2–H_2O exchange site is expressed as c_m (see Sects. "CO_2 exchange fluxes during photosynthesis" and "Mesophyll conductance").

[1]Institute for Marine and Atmospheric Research Utrecht, Utrecht University, Utrecht, The Netherlands. [2]Institute of Environmental Biology, Utrecht University, Utrecht, The Netherlands. [3]Meteorology and Air Quality Group, Wageningen University, Wageningen, The Netherlands. [4]Department of Earth Sciences, Utrecht University, Utrecht, The Netherlands. [5]Present address: Picarro B.V., 's-Hertogenbosch, The Netherlands. [6]These authors contributed equally: Getachew Agmuas Adnew and Magdalena E. G. Hofmann. ✉email: g.a.adnew@uu.nl

Laboratory studies have shown that the rate of exchange between CO_2 and water is the same for $\delta^{18}O$ and Δ_{47}[32,33]. This finding suggests that the equilibration between CO_2 and leaf water, soil water or open surface water should affect Δ_{47} with similar kinetics as $\delta^{18}O$, but in contrast to $\delta^{18}O$, Δ_{47} does not depend on the isotopic composition of the different water pools. The rapid isotope exchange of CO_2 with leaf and surface waters is thought to drive the Δ_{47} of atmospheric CO_2 towards the thermodynamic equilibrium value[1,19].

Measurements of Δ_{47} in CO_2 from air samples show that the clumped isotopic composition in the atmosphere is not in thermodynamic equilibrium at the global mean air temperature. For instance, background CO_2 from remote air observatories shows Δ_{47} values of 0.92 ‰[21], which is 0.06 ‰ lower than the expected value of 0.98 ‰ for a global mean air temperature of 15°C[34]. In urban and suburban air, Δ_{47} values are generally even lower and the variability of the reported Δ_{47} values was higher, possibly due to input from anthropogenic CO_2 formed in high temperature combustion. In Pasadena, Affek and Eiler[20], Affek, et al.[26], found Δ_{47} values between 0.73 and 1.01 ‰, and Eiler and Schauble[19] reported even lower values between 0.62 and 0.93 ‰ from a similar location. Laskar and Liang[22] reported Δ_{47} values between 0.75 and 0.93 ‰ for urban and suburban air in Taiwan.

Eiler and Schauble[19] developed a conceptual model to mathematically describe the effect of air-leaf interaction on the Δ_{47} signature of atmospheric CO_2. The main assumption is that the carbonic anhydrase catalyzed exchange between CO_2 and H_2O within the mesophyll will imprint a Δ_{47} value that reflects the effect of leaf temperature on the CO_2 that diffuses back out of the stomata to the atmosphere. In addition, kinetic fractionation during the diffusion into and out of the leaf through the stomata affects Δ_{47} during photosynthetic gas exchange. Eiler and Schauble[19] proposed that this kinetic isotope fractionation is significant especially for plant species that show a low carbonic anhydrase activity. In this case, the diffusive component during photosynthesis might lead to a depletion in Δ_{47} of atmospheric CO_2 of about 0.1 ‰ relative to the thermodynamic equilibrium value of CO_2–H_2O exchange alone.

Surprisingly, a recent study, Laskar and Liang[22] reported Δ_{47} measurements of CO_2 sampled in a greenhouse that show enrichment by up to 0.08 ‰ in Δ_{47} relative to the thermodynamic equilibrium value. The authors attributed this deviation to kinetic effects associated with the photosynthetic exchange, but as described in Eiler and Schauble[19], such a kinetic effect should lead to lower, not higher Δ_{47} values relative to the thermodynamic equilibrium. Furthermore Laskar and Liang[22] concluded that photosynthetic gas exchange would decouple Δ_{47} and $\delta^{18}O$ in contradiction to the simple CO_2–H_2O exchange model of Eiler and Schauble[19]. This discrepancy calls for controlled air-leaf gas exchange experiments to characterize the effect of photosynthesis on Δ_{47} in detail.

Here, we report results from photosynthetic gas exchange experiments under controlled conditions to quantify the effect of gas exchange on the isotopic composition of CO_2. We investigated the effect on Δ_{47} of the residual CO_2 (*i*) for different photosynthetic pathways (C_3 vs. C_4 plants), (*ii*) for two different values of leaf conductance in C_3 plants, and (*iii*) for variations in light intensities for one C_3 plant. This choice of plant species and gas exchange conditions enable us to directly test the proposed hypothesis proposed by Eiler and Schauble[19] that CO_2–H_2O exchange and kinetic fractionation with back-diffusion of CO_2 to the atmosphere are the main drivers controlling the Δ_{47} fractionation effect of photosynthetic gas exchange.

Materials and methods

Theory. *Background.* Δ_{47} describes the deviation of the abundance of $^{13}C^{18}O^{16}O$ (the dominant isotopologue with nominal mass 47) from the random distribution of all isotopes across all isotopologues in a CO_2 sample with the same bulk isotopic composition[24]. There are three isotopologues of CO_2 with nominal mass of 47, $^{13}C^{18}O^{16}O$ (abundance $= 46 \times 10^{-6}$), $^{17}O^{12}C^{18}O$ (abundance $= 1.6 \times 10^{-6}$) and $^{17}O^{13}C^{17}O$ (abundance $= 1.6 \times 10^{-9}$)[19]. The existing isotope ratio mass spectrometer instruments do not have sufficient mass resolving power to separate these isotopologues. Thus, the measured isotope ratio for nominal mass of 47 is a combination of these three isotopologues. Nevertheless, approximately 97% of the CO_2 with nominal mass 47 is $^{13}C^{16}O^{18}O$ and the Δ_{47} value is mostly referred to as the value of $^{13}C^{16}O^{18}O$ isotopologue. Δ_{47} is calculated as[19,35]:

$$\Delta_{47} = \frac{^{47}R}{^{47}R^*} - 1 \tag{1}$$

where R stands for the measured ratio of a rare isotopologue of the indicated mass to the most abundant isotopologue, and R^* is the isotopologue abundance ratio assuming that the heavy isotopes are distributed stochastically over all isotopologues[19,24]. In this case, $^{47}R^*$ can be calculated from the isotopologues of mass 44 and 47 as $^{47}R^* = [47]^*/[44]^*$ where $[44]^* = [^{12}C][^{16}O][^{16}O]$ and $47 = 2[^{13}C][^{16}O][^{18}O] + 2[^{12}C][^{17}O][^{18}O] + [^{13}C][^{17}O][^{17}O]$. Note that the factor 2 is a symmetry number. This leads to

$$^{47}R^* = \frac{2[^{13}C][^{16}O][^{18}O] + [^{13}C][^{17}O][^{17}O] + 2[^{12}C][^{17}O][^{18}O]}{[^{12}C][^{16}O][^{16}O]} = 2^{13}R^{18}R + 2^{17}R^{18}R + {}^{13}R(^{17}R)^2 \tag{2}$$

Measurements of both ^{13}R and ^{18}R (ratios $^{13}C/^{12}C$ and $^{18}O/^{16}O$) require solving Eq. 3.

$$-3K^2(^{18}R)^{2\lambda} + 2K^{45}R(^{18}R)^\lambda + 2^{18}R - {}^{46}R = 0 \tag{3}$$

where K is $^{17}R_{std}/(^{18}R_{std})^{\lambda}$[36] and λ is the three isotope exponent.

^{13}R and ^{18}R can be calculated from the corresponding δ values as ($^{13}R = (\delta^{13}C_{VPDB} + 1) \times 0.011180$, and $^{18}R = (\delta^{18}O_{VSMOW} + 1) \times 0.0020052$). It is impossible to measure ^{17}R of CO_2 directly with traditional gas source isotope ratio mass spectrometry due to the isobaric interference of $^{13}C^{16}O^{16}O$ on $^{12}C^{17}O^{16}O$. Variations in the isotope ratios ^{18}R and ^{17}R in a sample are closely linked in most common processes via the mass dependent fractionation equation $[^{18}R/^{18}R_{std}]^\lambda = {}^{17}R/^{17}R_{std}$ where *std* stands for standard[36]. In this study, a value of 0.528 is
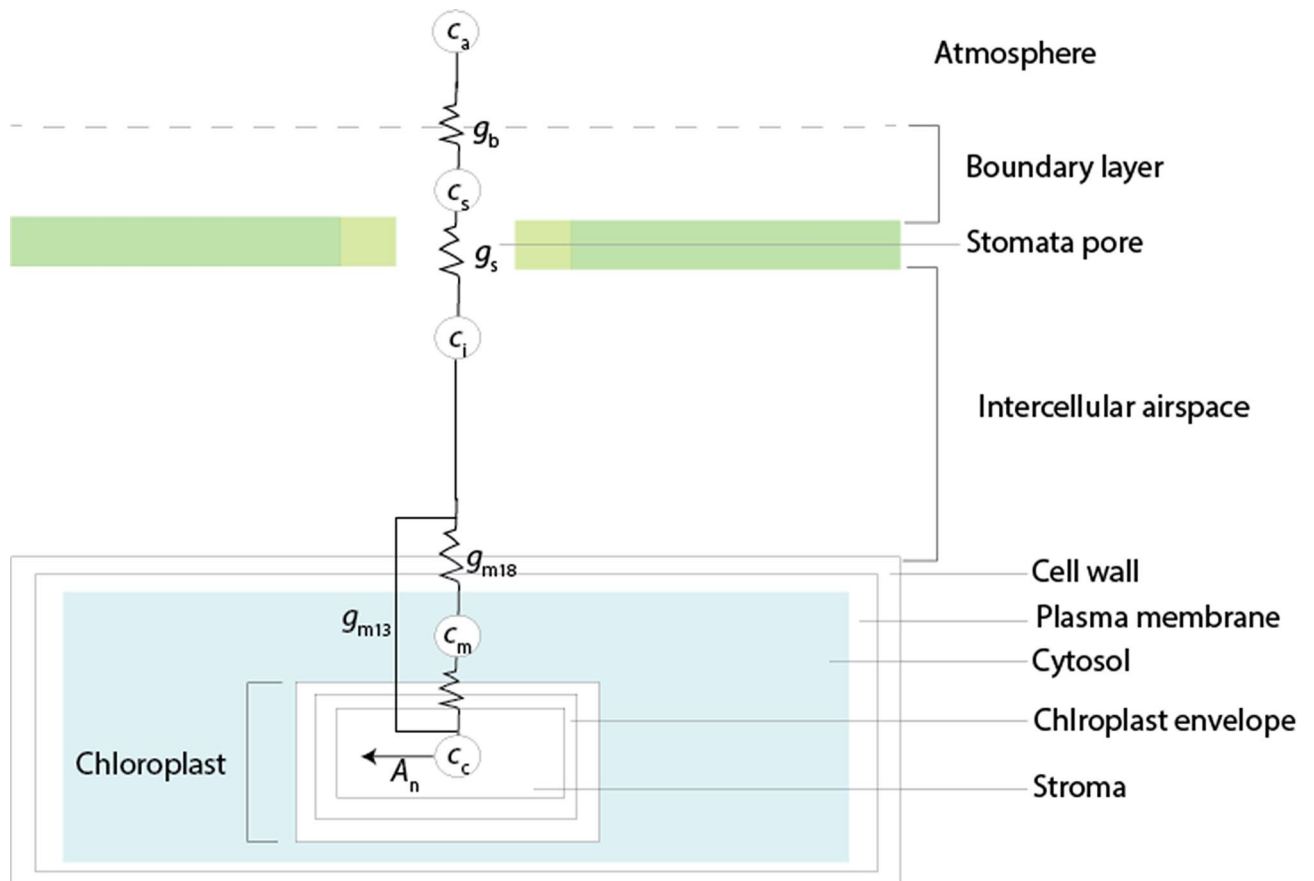
Figure 1. Schematic illustration of CO_2 exchange fluxes, concentrations and conductivities during photosynthetic gas exchange. Net photosynthetic CO_2 uptake in a leaf generates a concentration gradient over the leaf where c_a is the CO_2 concentration of the air, c_s the CO_2 concentration at the leaf surface, c_i is the CO_2 concentration in the intercellular air space, c_m is the CO_2 concentration in the mesophyll, i.e., the site of CO_2-H_2O exchange and c_c the CO_2 concentration in the chloroplasts, the site of CO_2 uptake. The g_b is the boundary layer conductance of CO_2 from the atmosphere to the leaf surface, the stomatal conductance g_s quantifies the gas exchange through the stomatal opening, g_{m13} is the mesophyll conductance to the site of carbon uptake and g_{m18} is the mesophyll conductance to the site of CO_2-H_2O exchange.

used as recommended by[37,38]. ^{17}R was calculated as $(^{17}R = \left(^{18}R/0.0020052\right)^{0.528} \times 0.0003799)$[35,37,38]. Recently, we have shown that ^{17}R can be measured independent of ^{13}C interference on O fragment ions[7].

$\delta^{13}C$ and $\delta^{18}O$ of the sample are calculated from δ^{45} and δ^{46} (i.e. $\delta^{13}C_{VPDB} \cong \delta^{45}_{sample} + 2 \times (^{17}R/^{13}R)_{VPDB\text{-}CO2} \times (\delta^{45}_{sample} - \lambda \times \delta^{45}_{sample})$ and $\delta^{18}O_{VPDB\text{-}CO2} \cong [\delta^{46}_{sample} - 0.0021 \times \delta^{13}C_{VPDB}]/0.99904)$, where $^{17}R/^{13}R$ is 0.03516[37]. The δ value is calculated as follow:

$$\delta^x = \left(\frac{^xR_{sample}}{^xR_{standard}} - 1 \right) \tag{4}$$

where x can be 13, 18, 45, 46 and 47 (for ^{13}C, ^{18}O, $^{13}C^{16}O^{16}O$, $^{12}C^{16}O^{18}O$ and $^{13}C^{16}O^{18}O$, respectively).

CO_2 exchange fluxes during photosynthesis. The CO_2 uptake by C_3 plants is schematically illustrated in Fig. 1. Net photosynthetic CO_2 uptake in a leaf generates a concentration gradient from the atmosphere (c_a) to the boundary layer (c_s), intercellular airspace (c_i), the mesophyll cell (c_m) and the chloroplast (c_c), where CO_2 is fixed (in C_3 plants) (see Fig. 1)[39–42]. In the chloroplast, the enzyme RubisCO catalyzes the conversion of carbon dioxide to the three-carbon acid 3-phosphoglyceric acid (3PGA). c_c determines the availability of CO_2 for carboxylation, which is the rate-limiting substrate. The concentration gradient between c_a and c_c drives the diffusion of CO_2 into the leaf. The diffusion process can be described mathematically following Fick's law of diffusion as:

$$A_n = g_L(c_a - c_c) \tag{5}$$

where g_L is the total conductance (inverse of resistance, $1/r_L$) of the leaf for CO_2 diffusion. Total g_L is conveniently subdivided into three parts that act in series. The boundary layer conductance (g_b) represents the conductance through a thin layer of near-stagnant air surrounding the leaf; it is a function of air turbulence and leaf area. The stomatal conductance (g_s) varies with the opening and frequency of the stomata. The mesophyll conductance

(g_m) quantifies the conductance for transport of CO_2 from the intercellular air space in the leaf to the site of CO_2–H_2O exchange in the mesophyll or the carboxylation in the chloroplast. The latter is expressed as g_{m13} and the former is denoted as g_{m18}, which refers to estimation using $\delta^{13}C$ and $\delta^{18}O$ respectively (see Sect. "Mesophyll conductance"). A small part of this transport occurs in the gas phase through a residual part of the intercellular air space. The major transport pathway is in the liquid phase, through the wall of the mesophyll cell, the plasmalemma and further into the cell to the site of oxygen exchange between CO_2 and H_2O that is catalyzed by carbonic anhydrase (CA). CO_2 diffuses further through the chloroplast envelope and into the chloroplast where carboxylation occurs[39,40,43].

Mesophyll conductance. For C_3 plants, we used the discrimination against ^{13}C ($\Delta_A{}^{13}C$) (Eq. 6) to estimate the mesophyll conductance (g_{m13}) from the intercellular airspace to the carboxylation site (Eq. 7) as described in[44]. The overall isotope fractionation associated with photosynthetic gas exchange is referred to as discrimination, which quantifies the enrichment or depletion of the isotope composition of CO_2 in the surrounding atmosphere relative to the CO_2 assimilated, see Eq. (6)[42,45,46]. Experimentally, the discrimination (Δ_A) is calculated from the isotopic composition and mole fraction of CO_2 entering and leaving the cuvette[47–49], as shown in Eq. (6).

$$\Delta_{Aobs}^x = \frac{\zeta\left(\delta_a^x - \delta_e^x\right)}{1 + \delta_a^x - \zeta\left(\delta_a^x - \delta_e^x\right)} \tag{6}$$

where x is either 13, 18 or 47 (for ^{13}C, ^{18}O and $^{13}C^{18}O^{16}O$ isotope composition, respectively), $\zeta = c_e/(c_e - c_a)$ and c is the mole fraction of the CO_2 entering (index e) and leaving (index a) the cuvette.

g_{m13} is calculated from the difference between the observed ^{13}C discrimination ($\Delta_A{}^{13}C_{obs}$) and the discrimination at infinite g_m ($c_i = c_c$) as:

$$g_{m13} = \frac{A_n/P}{c_i - c_c} = \left(\frac{1 + t^{13}}{1 - t^{13}}\right)\left(\frac{A_n\left(b - a_m - \frac{\alpha_b}{\alpha_e\alpha_R}e'\frac{R_D}{A_n}\right)}{\left(\Delta_A^{13}C_i - \Delta_A^{13}C_{obs}\right)Pc_a}\right) \tag{7}$$

where P is the ambient pressure, t^{13} is a ternary correction factor for $^{13}CO_2$, b the fractionation due to uptake by Rubisco, and a_m the combination of the fractionations associated with $^{13}CO_2$ dissolution and diffusion through water, respectively. e', R_D, α_e, and α_b are the fractionation factor for mitochondrial respiration including the apparent fractionation, the day respiration rate (mitochondrial respiration in the light) the fractionation factor for day respiration with respect to net assimilation and the fractionation factor for C_3 carboxylation, respectively. $\alpha_R = 1 + (R_D/A_n) \times (e'/\alpha_e)$. A detailed description of the equations, used parameters and definitions of fractionation factors is provided in Table S1 of the supplementary material.

In C_4 plants, the CO_2 is converted to bicarbonate and fixed to a four-carbon acid catalyzed by phosphoenol pyruvate carboxylase (PEPC) in the mesophyll. Unlike for C_3 plants, it is impossible to estimate mesophyll conductance from $\Delta_A{}^{13}C$ for C_4 plants due to the low photosynthetic fractionation[50,51]. However, the apparent discrimination against ^{18}O ($\Delta_A{}^{18}O$) can be used to estimate the mesophyll conductance from the intercellular air space to the site of CO_2–H_2O isotope equilibration, g_{m18}, as described in[41,47,52–54], for both C_3 and C_4 plants. The analytical expression for estimating g_{m18} (Eq. 8) assumes that the degree of equilibration between CO_2 and H_2O is 100%. Some studies have reported that the degree of equilibration can be lower than 100%, especially for C_4 plants, which have a lower CA activity[29,31,47,54]. Detailed information is provided in Table S1 of the supplementary material.

$$g_{m18} = \frac{A_n/P}{c_i - c_m} = \left(\frac{A_n/P}{c_i}\right)\frac{\delta^{18}O_A\alpha_{18w} + a_{18w} - \delta^{18}O_m}{\delta^{18}O_i - \delta^{18}O_m} \tag{8}$$

$\delta^{18}O_i$ is $\delta^{18}O$ of CO_2 in the intercellular airspace, α_{18w} is the fractionation factor for $^{12}C^{18}O^{16}O$ during diffusion and dissolution in water, a_{18w} is the discrimination against $^{12}C^{18}O^{16}O$ during diffusion and dissolution in water, $a_{18w} = \alpha_{18w} - 1$, $\delta^{18}O_A$ is $\delta^{18}O$ of the assimilated CO_2 and $\delta^{18}O_m$ is the $\delta^{18}O$ of CO_2 in equilibrium with leaf water at the CO_2–H_2O exchange site. In previous studies, the difference between $\delta^{18}O$ of bulk leaf water and the water at the evaporation site was about 1 to 2 ‰ higher[13,54], but larger differences have also been reported[55]. In this study, we assumed that the $\delta^{18}O$ of leaf water at the CO_2–H_2O exchange site is enriched by 2 ‰ compared to bulk leaf water and the degree of equilibration between CO_2 and leaf water is 100%.

Photosynthetic Δ_{47} discrimination. The effect of photosynthetic gas exchange on Δ_{47} depends on the assimilation rate, the various conductances mentioned before and the fraction of CO_2 that diffuses back to the atmosphere after isotope exchange with leaf water. For a laminar boundary layer, diffusion through the boundary layer decreases the Δ_{47} value of residual CO_2 by an amount equal to the boundary layer diffusive fractionation (+ 0.2 ‰) multiplied by the fraction of CO_2 enters leaves and is fixed (~ 1/3), i.e., 0.07 ‰. In this study, we used a fan (see Sect. "Leaf cuvette set-up"), which creates a turbulent boundary layer with an estimated conductance of 5 mol m^{-2} s^{-1}. The boundary layer conductance for the leaf cuvette was determined using wet filter paper from measurements of relative humidity and temperature of air in the cuvette as described in Parkinson[56]. As a result, the fractionation in Δ_{47} due to diffusion through the boundary layer is negligible compared to the precision of the measurement (ca. ~ 0.002 ‰). Figure 2 illustrates the effect of photosynthetic gas exchange on Δ_{47} for two extreme scenarios. The first "uptake dominated" scenario assumes that all the CO_2 entering stomata gets assimilated, leading to $c_m/c_a \sim 0$ whereas in the second "exchange dominated" scenario all CO_2 diffuses back to the atmosphere after exchange with the leaf water leading to $c_m/c_a \sim 1$. In the uptake dominated scenario, the result-
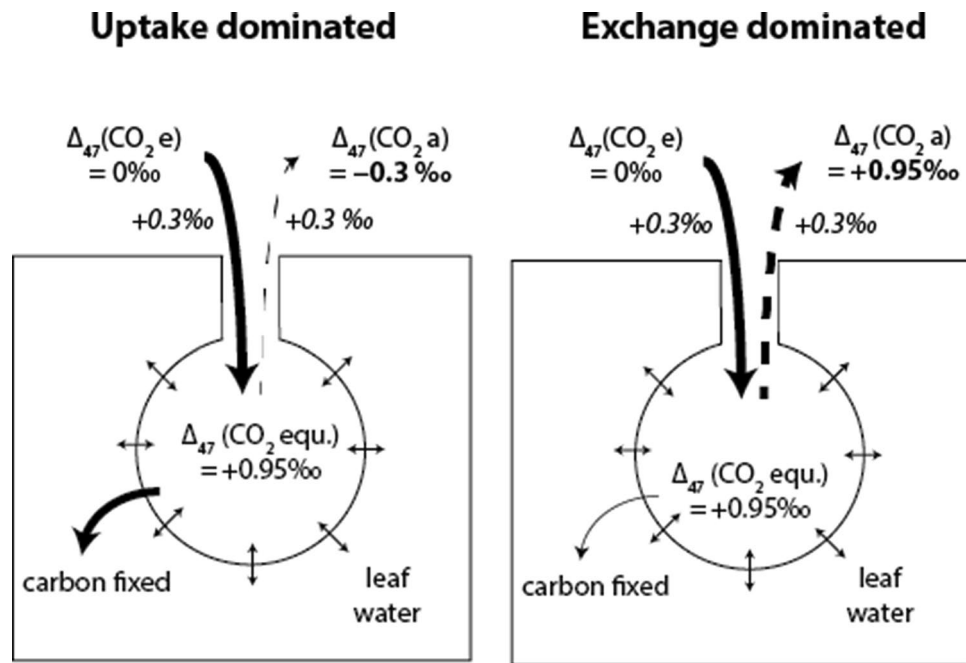
Uptake dominated

Exchange dominated

Figure 2. Schematic illustration of the clumped isotope fractionation during air-leaf gas exchange. Δ_{47} of the CO_2 in the air surrounding the leaf is mainly controlled by CO_2-H_2O exchange and kinetic fractionation during diffusion into and out of the leaf stomata. In the uptake dominated case ($c_m/c_a \sim 0$), -0.3 ‰ comes from the fact that diffusion mediated leaf air interaction will reduce the Δ_{47} value by 0.3 ‰, neglecting other effects. Diffusion only will reduce the Δ_{47} value by 0.3 ‰ multiplied by the fraction of CO_2 entering the leaf that is assimilated [19]. The boundary layer conductance is large and we have omitted it here.

ing Δ_{47} signal is mainly affected by diffusion, in the exchange dominated scenario the Δ_{47} signal is dominated by the CO_2–H_2O exchange. A similar scheme for $\delta^{18}O$ is shown in Figure S2 of the supplementary material.

The fractionation of Δ_{47} associated with photosynthetic gas exchange ($\Delta_A\Delta_{47obs}$) was calculated in a similar way as Δ_{Aobs}^x in Eq. (6) from the difference in CO_2 concentration and isotopic composition between the air entering and leaving the leaf cuvette (Eq. 9). For mixing of two different populations of CO_2, Δ_{47} is not a conserved quantity and the error introduced by adding or subtracting Δ_{47} values linearly depends on the relative difference in the $\delta^{18}O$ and $\delta^{13}C$ of the two gases[19,20,57,58]. In our study, the maximum difference between the $\delta^{18}O$ and $\delta^{13}C$ value of the CO_2 entering and leaving the cuvette is 14 ‰ and 4 ‰, respectively. For this rather small range, the error introduced due to linear addition and subtraction of Δ_{47} values of the CO_2 entering and leaving the cuvette is not significant (< 0.01 ‰).

$$\Delta_A\Delta_{47obs} = \frac{\zeta\,(\Delta_{47a} - \Delta_{47e})}{1 + \Delta_{47a} - \zeta(\Delta_{47a} - \Delta_{47e})} \tag{9}$$

Leaf cuvette model. To explore the effects of conductance, assimilation rate and back-diffusion of CO_2 to the atmosphere on the Δ_{47} of ambient CO_2 in detail we used a leaf cuvette model [https://git.wur.nl/leaf-model][59] that has been used for the interpretation of $\Delta^{17}O$ measurements in leaf exchange experiments recently[13]. In the model we assumed that CO_2–H_2O exchange in the mesophyll is rapid enough to constantly set Δ_{47} to thermodynamic equilibrium with the water, i.e., $\Delta_{47} = 0.95$ ‰ at 20 °C[25]. Thus, any change in bulk isotopic composition of CO_2 due to assimilation does not affect Δ_{47}[19]. Furthermore, CO_2 diffusion into and out of the intercellular air space through the stomata is associated with a fractionation constant of $+0.3$ ‰ for Δ_{47}[19] whereas CO_2 diffusion through the boundary layer has a fractionation constant of $+0.2$ ‰ for Δ_{47}.

The steady state model considers five compartments: (i) atmosphere (air in the leaf surrounding), (ii) the leaf surface, (iii) the intercellular airspace of the leaf, (iv) the mesophyll cell of the leaf, and (v) the chloroplast (see Fig. 1). The air enters the leaf cuvette at a flow rate F_e and a CO_2 concentration c_e with a well-defined isotopic composition δ_e (where δ can stand for $\delta^{13}C$, $\delta^{18}O$, δ^{47} and Δ_{47}, see Sect. "Background" for definition). The leaf inside the cuvette takes up a portion of the CO_2 and this uptake is associated with an isotope fractionation. The air flowing out of the cuvette has flow rate F_a, CO_2 concentration c_a and isotopic composition δ_a. The photosynthetic uptake in the chloroplasts leads to a concentration gradient between the air surrounding the leaf and the chloroplasts so that there is a net flow of CO_2 from the cuvette into the intercellular airspace, to the mesophyll cell, and finally to the chloroplasts. The corresponding CO_2 concentrations decrease accordingly in the order c_a, c_s, c_i, c_m and c_c. Diffusion, isotopic equilibration with H_2O, CO_2 uptake and mixing between the model reservoirs lead to a change in isotopic composition (δ_a, δ_s, δ_i, δ_m and δ_c). The magnitude of the exchange fluxes between the
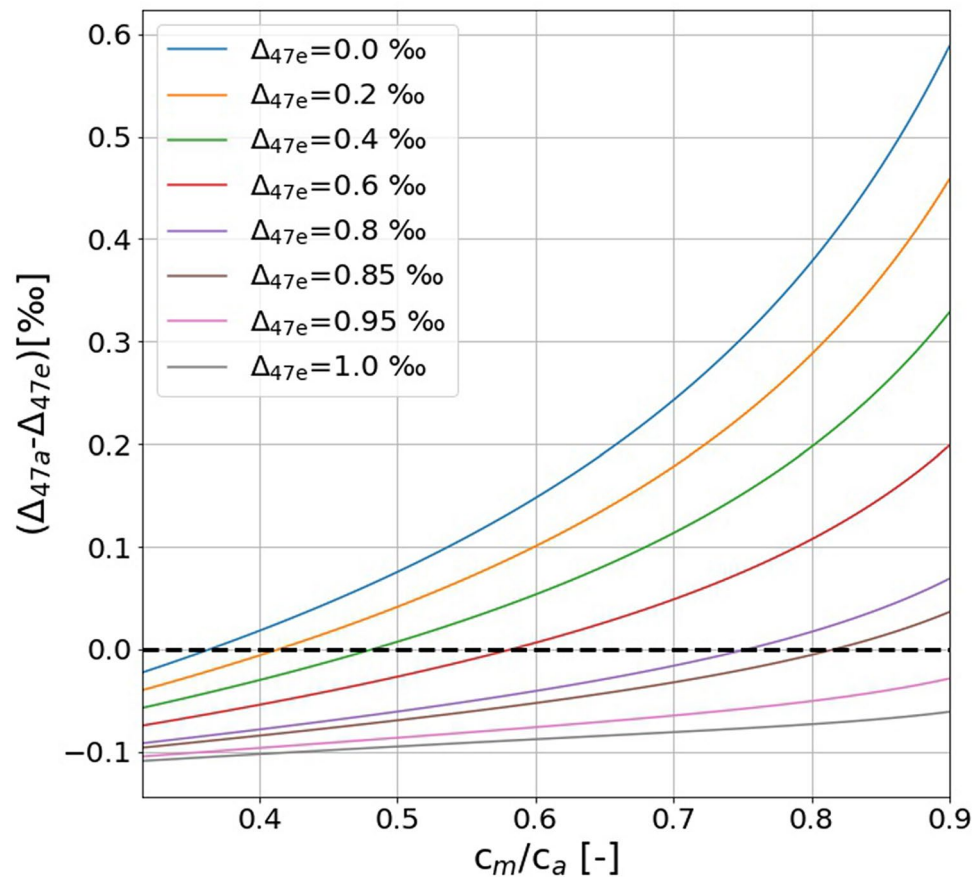
Figure 3. Difference between Δ_{47} of out- and inflowing CO_2 as function of the fraction of CO_2 diffusing back to the atmosphere (c_m/c_a) calculated with the leaf cuvette model. The black dashed line shows the c_m/c_a ratio where the Δ_{47} relative difference between the ingoing and outgoing CO_2 becomes zero for the corresponding Δ_{47} of CO_2 entering the cuvette.

compartments is defined by the boundary layer conductance g_b, stomatal conductance g_s and the mesophyll conductances g_{m18} and g_{m13}. In the leaf cuvette model, the boundary layer conductance g_b is assumed 5 mol m^{-2} s^{-1}, similar to the value determined in the experiment.

Figure 3 shows how the Δ_{47} value changes between incoming and outgoing CO_2 in the leaf cuvette model for c_m/c_a ratios ranging from 0.3 to 0.9 and Δ_{47} values of the entering CO_2 between 0.0 ‰ and 1.0 ‰. It is evident that the relative changes are small when Δ_{47} of the incoming CO_2 is close to the equilibrium value (0.9—1.0 ‰) at ambient temperatures. The changes are much larger if the Δ_{47} of the incoming CO_2 is close to a random distribution ($\Delta_{47} = 0.0$ ‰). This motivated us to carry out the gas exchange experiments with isotopically 'scrambled' (i.e., Δ_{47} close to zero) CO_2 (see below).

Plant material and growth conditions. Three plant species were used for the experiments, belonging to different functional groups: Sunflower (*Helianthus annuus* L. cv, Giganteus), Atlantic ivy [*Hedera hybernica* (Kirchner) Bean (syn. *Hedera helix* var. hibernica)], and maize (*Zea mays* L. cv, Torres). The fast-growing annual C$_3$ species *Helianthus* is characterized by short-lived leaves with high photosynthetic capacity and conductance for CO_2 diffusion. The other C$_3$ species, the evergreen *Hedera*, has long-lived leaves with a lower photosynthetic capacity and conductance. The third species, *Zea*, has C$_4$ metabolism, a high photosynthetic capacity and low conductance.

Helianthus and *Zea* were grown from seed in a growth room at 20 °C, a relative humidity of 70% and a photosynthetic photon flux density (PPFD) of 250 µmol m^{-2} s^{-1} for a day length of 16 h. The first pair of two leaves of *Helianthus* was used for the experiments when fully grown at three to four weeks after planting. Younger leaves that shaded them were removed. For *Zea mays*, a section of the fifth or sixth leaf at about two thirds of total leaf length was used at a plant age of around 7 weeks. These leaves were about 5 cm wide, giving a sufficiently large leaf area in the cuvette. *Hedera* plants were obtained from a grower, pruned to reduce self-shading and further grown in the experimental garden in full daylight. They were used for the experiments in early November 2015 when outside average maximum day temperature during the preceding month was 14 °C. Mature leaves that could be accommodated intact in the cuvette were used for the experiments. For all the experiments, leaves
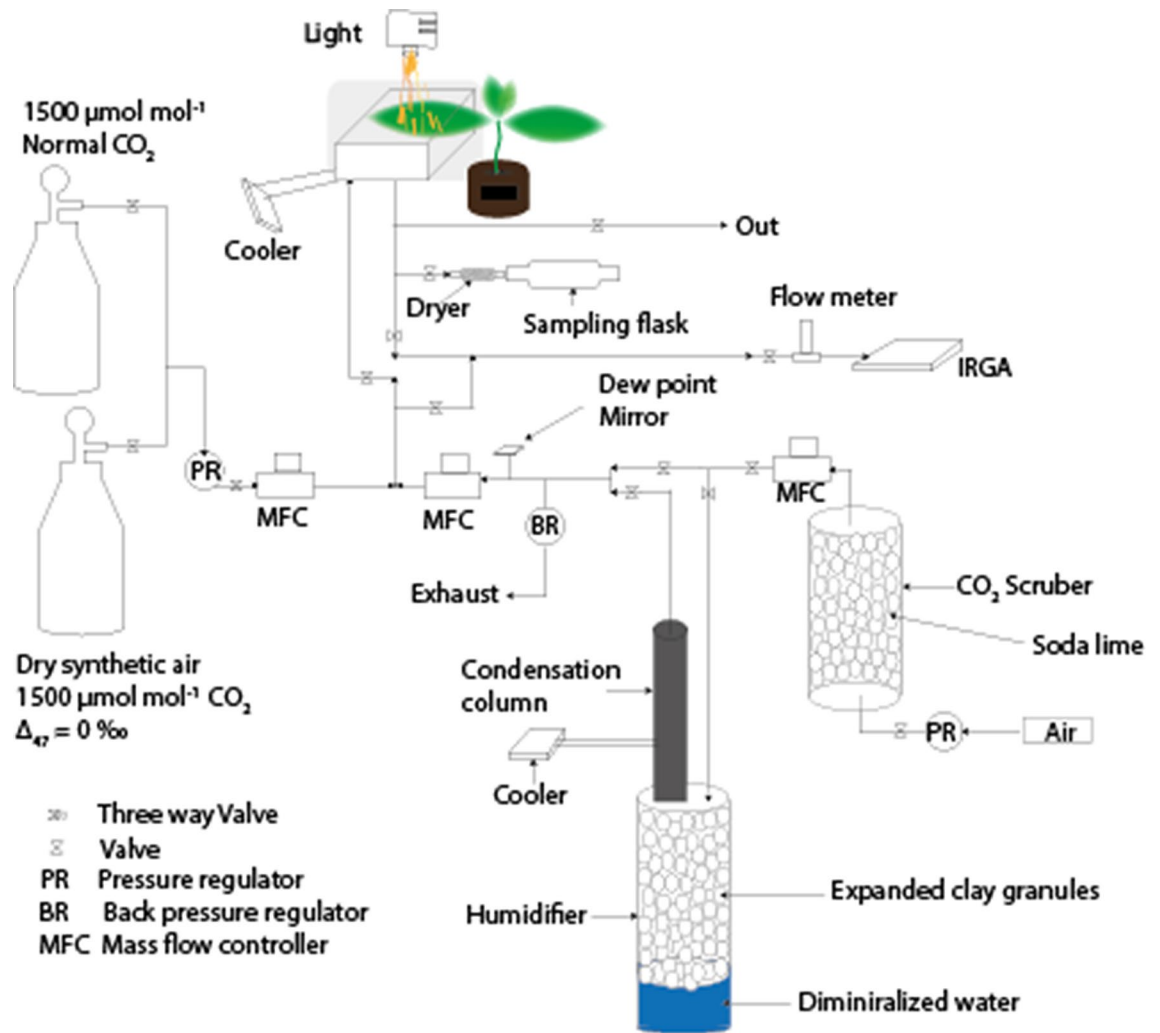
Figure 4. Leaf chamber set-up, modified from Adnew et al. (2020)[13]. A single leaf was placed in the leaf cuvette and the light intensity could be regulated to manipulate the assimilation rate. A gas-mixing unit was used to mix dry synthetic air with scrambled CO_2 with humidified CO_2-free air to obtain an overall CO_2 concentration of the ingoing air of 500 µmol mol^{-1}. The flow rate was adjusted to the photosynthetic activity of the leaf to obtain a CO_2 concentration of about 400 µmol mol^{-1} at the outlet (0.6 to 1.5 L min^{-1}). CO_2 and H_2O concentrations were monitored with an infrared gas analyzer (IRGA). Once steady state was reached, the outgoing air was sampled in one 2 L and one 1 L glass flasks, in series. The bulk isotope composition ($\delta^{13}C$ and $\delta^{18}O$) of the normal CO_2 and scrambled CO_2 are identical.

remained attached to the plants during the experiments. Both *Helianthus* and *Zea* are watered from tap water whereas *Hedera* received largely rain water.

Leaf cuvette set-up. The isotopic effect of CO_2 exchange during photosynthesis was investigated with an open gas exchange measurement system similar to the one described by[13,60] (Fig. 4). A controlled flow of air entered and left the leaf cuvette, which had a 7×7 cm transparent window on top that limited the maximum width of the leaves that could be accommodated. A fan inside the leaf cuvette increased boundary layer conductance to around 5 mol m^{-2} s^{-1} and mixed the air thoroughly so that the air leaving the cuvette was a representative sample of the air inside. The chamber was illuminated from above by a halogen lamp that allowed control of the PPFD incident on the leaf. Leaf temperature was measured with thermocouples appressed to the abaxial side of the leaf. Water at 20 °C was circulated through the double wall of the cuvette, which stabilized leaf temperature up to 3 °C higher depending on PPFD and transpiration rate (Table 1).

A gas-mixing unit made from ¼ inch stainless-steel tubing was attached to the inlet port of the cuvette. Synthetic dry air with a CO_2 concentration of about 1500 µmol mol^{-1} was mixed with CO_2-free air of controlled humidity to set the CO_2 concentration of inlet air to 500 µmol mol^{-1}. Air flows were controlled with flow controllers. Two of these mixing units were used, one with untreated CO_2 and the other one with the same CO_2 that was previously isotopically scrambled at 1000 °C (target $\Delta_{47} \sim 0.0$ ‰, see below for discussion of deviations). The air flow rate was adjusted so that the CO_2 concentration at the outlet (and thus also in the cuvette) was about

Species	Leaf type	PPFD $\frac{\mu mol}{m^2 s}$	No. exp	T_{leaf} [°C]	$c_e \frac{\mu mol}{mol}$	$c_a \frac{\mu mol}{mol}$	$A_n \frac{\mu mol}{m^2 s}$	$E \frac{mmol}{m^2 s}$	$g_s \frac{mol}{m^2 s}$	$g_{m13} \frac{mol}{m^2 s\,bar}$	$g_{m18} \frac{mol}{m^2 s\,bar}$	c_i/c_a	c_c/c_a	c_m/c_a	$\delta^{18}O_{LW}$
H.ann-uus	C_3	200	(1)	21.4	499	420	12.0	2.3	0.27	0.33 ± 0.05	0.59 ± 0.05	0.80	0.71 ± 0.02	0.75 ± 0.01	4.3 ± 0.1
			(2)	21.2	499	406	12.2	2.6	0.32	0.17 ± 0.05	0.82 ± 0.05	0.81	0.64 ± 0.02	0.78 ± 0.03	6.0 ± 0.1
			(3)	20.6	501	409	11.3	2.1	0.35	0.36 ± 0.05	0.64 ± 0.05	0.85	0.78 ± 0.02	0.81 ± 0.01	6.5 ± 0.1
			Mean ± SD	**21.1 ± 0.4**	**500 ± 1**	**412 ± 7**	**11.8 ± 0.5**	**2.3 ± 0.3**	**0.31 ± 0.04**	**0.27 ± 0.1**	**0.68 ± 0.12**	**0.82 ± 0.03**	**0.71 ± 0.07**	**0.78 ± 0.03**	**5.6 ± 1.2**
		700	(4)	21.8	500	399	24.4	4.1	0.51	0.61 ± 0.05	0.93 ± 0.05	0.78	0.68 ± 0.02	0.71 ± 0.01	4.7 ± 0.1
			(5)	22.2	499	406	20.9	3.0	0.33	0.46 ± 0.05	0.67 ± 0.05	0.74	0.63 ± 0.02	0.66 ± 0.01	6.1 ± 0.1
			(6)	21.3	500	404	20.8	3.5	0.45	0.43 ± 0.05	0.52 ± 0.05	0.79	0.67 ± 0.02	0.69 ± 0.01	6.6 ± 0.1
			(7)	21.4	499	405	20.7	3.7	0.45	0.65 ± 0.05	0.72 ± 0.05	0.79	0.71 ± 0.02	0.72 ± 0.01	6.5 ± 0.1
			Mean ± SD	**21.7 ± 0.4**	**500 ± 1**	**404 ± 3**	**21.7 ± 1.8**	**3.6 ± 0.5**	**0.44 ± 0.08**	**0.54 ± 0.1**	**0.71 ± 0.17**	**0.78 ± 0.02**	**0.67 ± 0.03**	**0.70 ± 0.03**	**6.0 ± 0.9**
		1800	(8)	23.7	500	401	27.8	5.4	0.53	0.46 ± 0.05	0.81 ± 0.05	0.74	0.59 ± 0.02	0.66 ± 0.01	6.7 ± 0.1
			(9)	23.8	502	411	22.2	4.5	0.39	0.45 ± 0.05	0.55 ± 0.05	0.73	0.62 ± 0.02	0.64 ± 0.01	6.9 ± 0.1
			(10)	22.9	501	405	23.5	4.5	0.55	0.37 ± 0.05	0.59 ± 0.05	0.79	0.63 ± 0.02	0.69 ± 0.01	5.9 ± 0.1
			Mean ± SD	**23.5 ± 0.5**	**501 ± 1**	**406 ± 5**	**24.5 ± 2.9**	**4.8 ± 0.5**	**0.49 ± 0.09**	**0.43 ± 0.05**	**0.65 ± 0.14**	**0.75 ± 0.03**	**0.61 ± 0.02**	**0.66 ± 0.03**	**6.5 ± 0.5**
H. Hibernica	C_3	700	(1)	22.6	499	404	15.2	1.2	0.08	0.21 ± 0.05	0.36 ± 0.05	0.41	0.23 ± 0.02	0.30	2.4 ± 0.1
			(2)	22.8	500	395	14.8	1.0	0.08	0.17 ± 0.05	0.24 ± 0.05	0.41	0.20 ± 0.02	0.26	1.9 ± 0.1
			(3)	22.7	498	395	15.8	1.3	0.09	0.21 ± 0.05	0.31 ± 0.05	0.42	0.23 ± 0.02	0.29	4.9 ± 0.1
			Mean ± SD	**22.7 ± 0.1**	**499 ± 1**	**398 ± 5**	**15.3 ± 0.5**	**1.2 ± 0.2**	**0.08 ± 0.01**	**0.20 ± 0.02**	**0.30 ± 0.06**	**0.41 ± 0.01**	**0.22 ± 0.02**	**0.28 ± 0.02**	**3.1 ± 1.6**
Z. mays	C_4	700	(1)	22.0	501	404	28.2	1.8	0.11	–	0.65 ± 0.05	0.23	–	0.12	19.3 ± 0.1
			(2)	21.8	499	411	29.2	1.9	0.12	–	0.58 ± 0.05	0.26	–	0.14	20.3 ± 0.1
			(3)	22.0	501	401	26.7	1.7	0.16	–	0.49 ± 0.05	0.48	–	0.35	21.9 ± 0.1
			Mean ± SD	**21.9 ± 0.1**	**500 ± 1**	**405 ± 5**	**28 ± 1.3**	**1.8 ± 0.1**	**0.13 ± 0.03**		**0.57 ± 0.08**	**0.32 ± 0.14**		**0.20 ± 0.13**	**20.5 ± 1.3**

Table 1. Gas exchange variables and isotopic composition of the bulk leaf water. T_{leaf}: leaf temperature; c_e: CO_2 concentration of the air entering the leaf cuvette; c_a: CO_2 concentration of the air inside the cuvette and leaving the cuvette; A_n: net assimilation rate; E: transpiration rate; g_s: stomatal conductance for CO_2; c_i: CO_2 concentration in the intercellular airspace; c_c: CO_2 concentration in the chloroplasts (site of CO_2 uptake); c_m: CO_2 concentration in the mesophyll cell; g_{m13}: mesophyll conductance from the intercellular airspace to the chloroplasts; g_{m18}: mesophyll conductance from the intercellular airspace to the CO_2-H_2O exchange site; $\delta^{18}O_{LW}$: $\delta^{18}O$ value of the bulk leaf water vs VSMOW (‰). The values in bold are mean and standard deviation for the replicates at different light conditions.

400 µmol mol^{-1}. Thus, the decrease in CO_2 concentration in the cuvette as a result of uptake by the leaf was about 100 µmol mol^{-1}. In typical experiments the air flow rate was between 0.6 and 1.5 L min^{-1} depending on the CO_2 uptake rate of the leaf. It generally took 1 h to reach steady state gas exchange conditions. Gas exchange was measured before and after sampling with an infrared gas analyzer (IRGA) (LI-6262; Li-Cor, Lincoln, NE, USA) operated in the absolute mode. CO_2 and H_2O concentrations of inlet and outlet air were measured subsequently. The IRGA used for CO_2 mole fraction measurements, was calibrated every day with compressed air (dry) which has a known CO_2 mole fraction, and the reference cell was flushed with CO_2-free N_2 gas. For the water mole fraction, the IRGA was calibrated using a dew point mirror, and the reference cell was flushed with CO_2-free N_2 gas. Gas exchange variables were calculated according to von Caemmerer and Farquhar [61] (see supplementary material Table S1).

The measurements before and after sampling were used to check whether leaves remained sufficiently in steady state over the sampling period, if not, the samples were discarded. The mean value of the two gas exchange measurements (before and after collecting an air sample) were used to calculate the gas exchange parameters. Preparing scrambled CO_2 is labor intensive, as a result we used normal CO_2 during the gas exchange experiment until reaching steady state. After the steady state was reached (i.e. constant CO_2 and H_2O mole fractions) the CO_2 source was switched to the scrambled CO_2 supply (Fig. 4) and we waited 15 min to re-establish steady state conditions. Sampling of air was done by attaching a $Mg(ClO_4)_2$ dryer (Sigma Aldrich, USA) and 6-L of glass flasks to the outlet of the cuvette. The duration of completely flushing and filling the flasks depended on the flow rate and varied between 20 and 50 min.

We regularly determined the isotopic composition of the entering CO_2 by flushing it through an empty leaf cuvette and sampling the air at the outlet as a blank experiment. We used two different synthetic air cylinders spiked with scrambled CO_2: The first cylinder had a $\delta^{13}C$ value of − 2.50 ± 0.02 ‰, a $\delta^{18}O$ value of 25.3 ± 0.1 ‰ and a Δ_{47} value of 0.24 ± 0.02 ‰; the second cylinder had a $\delta^{13}C$ value of − 2.43 ± 0.03 ‰, a $\delta^{18}O$ value of 25.5 ± 0.2 ‰ and a Δ_{47} value of 0.07 ± 0.03 ‰ (Table S1, supplementary material). If not indicated differently, these and all further errors reported in this manuscript are 1 σ standard deviation, determined from repeated analysis of samples.

Automated CO_2 extraction from air. We used an automated CO_2 extraction and purification system to prepare the sample CO_2 for $^{13}C^{18}O^{16}O$ analysis. The system was mainly manufactured from stainless steel parts and consisted of four main units: (i) an air inlet system, (ii) chemical and cryogenic CO_2 drying units, (iii) a
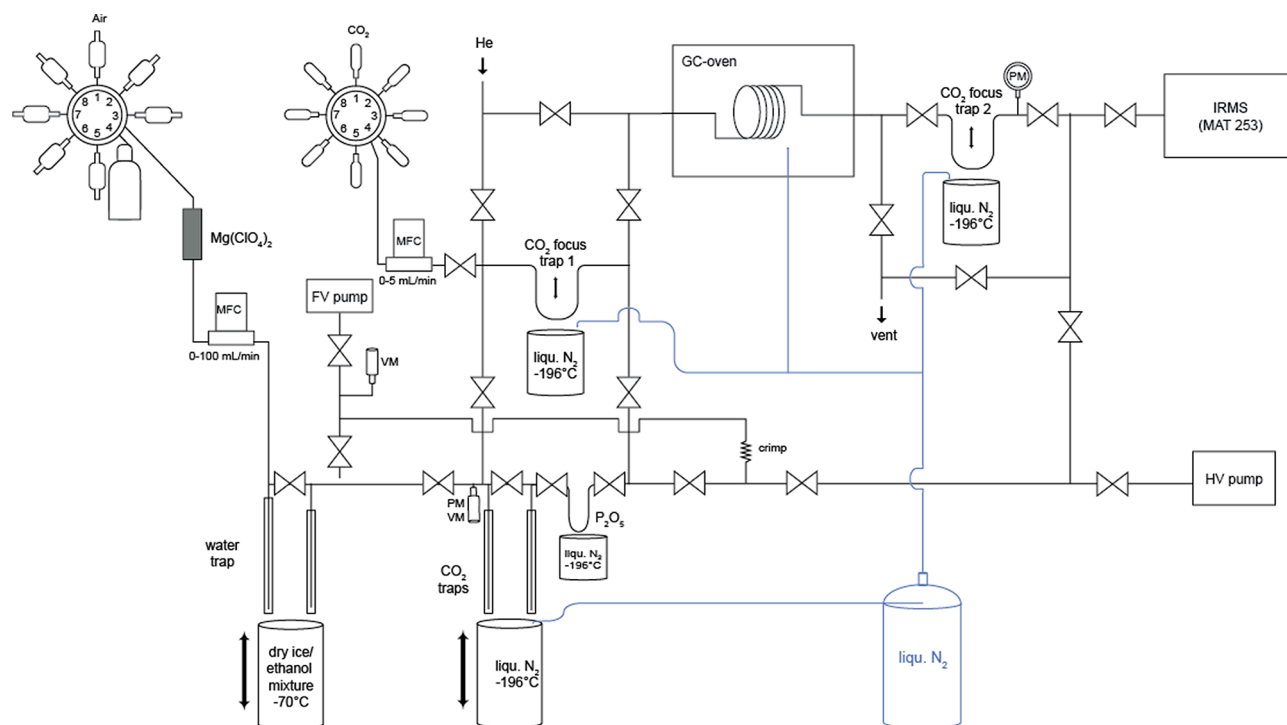
Figure 5. Schematic of the automated system for CO_2 extraction from air and purification system. The liquid nitrogen tank is connected to the Dewar using Teflon tube covered with a temperature insulator.

cryogenic CO_2 trap and (iv) a GC column for purification (Fig. 5). The outlet of the extraction line was directly connected to the sample bellows of the mass spectrometer. The design of the air inlet system and the cryogenic water and CO_2 traps were based on an automated CO_2 extraction system dedicated to conventional mass spectrometric isotope analysis of atmospheric CO_2[62].

The air inlet system allowed connecting several air samples via an 8-port Valco multiport valve: One position of the multiport valve was capped off and was used as a 'closed' position, two positions were generally used for working gas cylinders and the remaining five positions could be used to connect the sample flasks. About 2.5 L of air were required for one analysis. For a few samples we measured duplicates. Prior to an extraction sequence, the analytical system was evacuated up to the flask valves. The outlet of the multiport valve was connected to a mass flow controller ($10-100$ mL min^{-1}; MKS Instruments) to regulate the gas flow during the extraction system. The flow rate was routinely set to 50 mL min^{-1} for extracting the CO_2 from air.

In order to minimize exchange with water the gas was thoroughly dried at three different positions in the automated extraction system: (i) before the mass flow controller with a magnesium perchlorate unit, (ii) after the mass flow controller with two cryogenic water traps, and (iii) after the CO_2 trap with a phosphorus pentoxide (P_2O_5) unit. The magnesium perchlorate was filled in a ca. 10 cm long open-end glass tube with 10 mm inner diameter in the central part and ¼" connectors. The drying agent was held in place with glass wool. The cryogenic water traps were made from 25 cm long stainless steel tubes with a diameter of ¼" and inner tubes with a diameter of 1/8"[63]. The outer tubes were welded tight at the bottom and electropolished afterwards to reobtain a smooth surface. The inner tubes ended about 0.5 cm above the bottom of the outer tubes to force the air through the entire length of the water trap. To enhance the cold transfer between the outer and inner tube, the inner tubes were slightly bent to touch the outer tubes. The cryogenic water traps were cooled with a mixture of dry ice and ethanol to -72 °C. The position of the Dewar with the cooling bath was controlled with a hydraulic lift. Due to the relatively large size of the Dewar, the temperature of the cooling bath stayed constant overnight. The (P_2O_5) drying unit consisted of a 10 cm long and 6 mm o.d. wide glass finger containing phosphorous pentoxide (P_2O_5), which was connected via a 1/8" stainless steel tube to the CO_2 trap. It was immersed in liquid nitrogen using a hydraulic lifter.

The chemical drying units were added to the system at a later stage in an attempt to reduce isotopic re-equilibration during the extraction process (see below). However, also these additional measures did not prevent partial re-equilibration in the extraction line so that we had to correct all Δ_{47} data for this partial re-equilibration. The size of the corresponding correction was established by frequently analyzing heated and non-heated CO_2 in air standards (see Sect. "Isotopic analysis of CO_2 (δ^{13}C, δ^{18}O and Δ_{47}").

Carbon dioxide (and nitrous oxide) was trapped by immersing the CO_2 trap in liquid nitrogen. The design of the carbon dioxide trap and cooling unit was the same as the cryogenic water trap described above. During extraction, the air was processed through the system with a fore vacuum pump. A mechanical flow restriction (crimped 1/16" stainless steel tubing) after the CO_2 trap slowed down the flow rate in the CO_2 trap. The crimping was adjusted such that the pressure in the water and CO_2 trap was about 180 mbar at a flow rate of 50 mL min^{-1}.

After trapping the CO_2 in the liquid nitrogen trap, the trap was warmed up to room temperature and the sample CO_2 was frozen to the P_2O_5 trap. Then, the valve on top of the P_2O_5 glass finger was closed and the CO_2 was brought to room temperature for final drying for about 10 min. Afterwards, the CO_2 was transferred to a 1/16″ focusing trap in front of the gas chromatographic column, by immersing this focusing trap in liquid nitrogen. The CO_2 was then released into a helium stream at a flow rate of approx. 25 mL min^{-1} through the gas chromatographic (GC) column packed with Porapak Q. The GC column was cooled to 20 °C during purification with cold nitrogen gas provided from a liquid nitrogen Dewar, to hold back possible hydrocarbon impurities[20] and it was heated up to 250 °C in-between extractions. After passing through the GC column, the CO_2 was trapped in a second 1/16″ trap and the helium was evacuated using the fore and high vacuum pump of the isotope ratio mass spectrometer (IRMS). Finally, the pure CO_2 was warmed to room temperature and injected into the mass spectrometer.

The whole CO_2 extraction line (including the liquid nitrogen cooling) was controlled via LabVIEW (Version 15.0). The LabVIEW software also gave a signal to the IRMS software Isodat (Version 2.0) to start a measurement. Extraction and purification of one sample took about 4.5 h and we generally analyzed two working standards and three samples per day.

Isotopic analysis of CO_2 ($\delta^{13}C$, $\delta^{18}O$ and Δ_{47}).

Mass spectrometric analysis of the isotopic composition of the extracted and purified CO_2 was carried out in dual inlet mode on a MAT 253 mass spectrometer (Thermo Fisher Scientific, Germany) with a modified collector unit that allowed simultaneous analysis of the mass-to-charge ratios (m/z) 44, 45, 46, 47, 48 and 49. The overall reproducibility for Δ_{47} analysis was about 0.04 ‰, determined from replicate measurements of the compressed air cylinder.

The mass spectrometric Δ_{47} measurements were calibrated relative to CO_2 heated to 1000 °C and CO_2 equilibrated with water at 28°C[25,64]. We analyzed heated and water equilibrated CO_2 with a different bulk isotopic composition and determined a slope of 0.0024 for the heated and water-equilibrated gas line (Figure S3, supplementary material). This slope was used to correct for small, negative background effects on m/z 47. The bulk isotopic composition of our in-house reference CO_2 gas was $\delta^{13}C_{VPDB} = -2.82$ ‰ and $\delta^{18}O_{VSMOW} = -26.11$ ‰ and the maximum δ^{47} difference between the sample and the reference CO_2 was 17 ‰ resulting in a maximum Δ_{47} bulk isotope composition effect -0.04 ‰ which is corrected based on heated and equilibration gas slope.

In order to calibrate our $\delta^{13}C$, $\delta^{18}O$ and Δ_{47} measurements of CO_2 in air, we prepared two cylinders of CO_2 in synthetic air as working reference cylinders (Table S2). The first synthetic air cylinder was spiked with CO_2 resulting in a concentration of about 500 µmol mol^{-1}, $\delta^{13}C_{VPDB} = -2.76$ ‰, $\delta^{18}O_{VSMOW} = 25.65$ ‰ and $\Delta_{47} = 0.82$ ‰. For the second synthetic air cylinder we used scrambled CO_2 with a similar bulk isotopic composition, i.e. $\delta^{13}C_{VPDB} = -2.73$ ‰, $\delta^{18}O_{VSMOW} = -25.83$ ‰ but a low clumped isotope signature of $\Delta_{47} = 0.11$ ‰ and a CO_2 concentration of 400 µmol mol^{-1}.

The clumped isotopic composition of the first air cylinder was determined by analyzing the pure CO_2 directly in the dual inlet system of the IRMS versus the heated and water equilibrated CO_2 samples and versus CO_2 obtained by acid digestion at 70 °C from a set of clumped isotope carbonate standards (ETH1, ETH2, ETH3 and ETH4). Both procedures gave consistent results of $\Delta_{47} = 0.82 \pm 0.04$ ‰. The same CO_2 was then mixed in reference air cylinder 1 with synthetic air. After extracting and purifying the CO_2, we found an average Δ_{47} value of 0.86 ± 0.04 ‰. The reason for this offset of 0.04 ± 0.04 ‰ might be partial re-equilibration within the extraction line, where full equilibration at room temperature would result in $\Delta_{47} = 0.93$ ‰.

For preparing the second air cylinder, we heated the pure CO_2 to 1000 °C for more than 2 hours[64] and then mixed it into synthetic, CO_2-free air. After extracting and purifying the CO_2 from the second cylinder, we determined an average Δ_{47} value of 0.42 ± 0.04 ‰. The reason for this significant deviation from the expected Δ_{47} value of 0.03 ‰ is most likely twofold: (i) partial re-equilibration during mixing of scrambled CO_2 with synthetic air, and (ii) partial re-equilibration in the automated CO_2 extraction line. Subsequently, we prepared several other mixtures of heated CO_2 with an expected clumped isotope signature of $\Delta_{47} = 0.03$ ‰ in synthetic air cylinders. For all cylinders that were prepared this way we found Δ_{47} values that were at least $+0.26$ ‰ enriched in Δ_{47} relative to the expected value. It is not straightforward to decide whether the clumped signal of a CO_2-in-air standard was altered during the preparation of the air standard or during the CO_2 extraction step. Comparison between the Δ_{47} of the pure CO_2 and Δ_{47} value after processing the CO_2-air mixtures through the CO_2 extraction line reveals a Δ_{47} scale contraction of 24%, i.e. we measure only 76% of the true difference between samples when determining the clumped isotopic composition of CO_2 in air. This apparent scale contraction was highly reproducible over the course of the experiments reported here and we corrected all Δ_{47} values accordingly. This illustrates that referencing Δ_{47} measurements for atmospheric CO_2 samples is challenging because there is no Δ_{47} standard for CO_2-in-air studies available.

The leaf gas exchange samples contained up to about 0.3 µmol mol^{-1} N_2O. All CO_2 isotope measurements of $\delta^{13}C$, $\delta^{18}O$ and Δ_{47} were corrected for the mass interference from the N_2O isotopologues because N_2O was not separated from CO_2 during the purification step. The amount of N_2O was inferred from the intensity of the N fragment at m/z 14 relative to the intensity of m/z 44[20]. For typical N_2O mole fractions of 0.3 µmol mol^{-1}, the N_2O correction was approximately $+0.17$ ‰ for $\delta^{13}C$, $+0.45$ ‰ for $\delta^{18}O$ and -0.13 ‰ for Δ_{47}.

Considering all correction procedures, most notable the 24% Δ_{47} scale contraction, we obtain an overall reproducibility for repeated extraction of CO_2 from air and subsequent isotopic analysis of 0.08 ‰ for $\delta^{13}C$, 0.3 ‰ for $\delta^{18}O$ and 0.045 ‰ for Δ_{47}.

Leaf water extraction and $\delta^{18}O$ analysis.

Immediately after sampling of air for Δ_{47} measurements, the leaf was placed between plastic sheets, its area was measured, and it was enclosed in a vial and frozen. Leaf water was extracted from the leaves by cryogenic vacuum distillation, i.e. the leaf sample was heated in vacuum

Species	PPFD	No. exp	Cyl	$\delta^{13}C_e$	$\delta^{13}C_a$	$\Delta_A{}^{13}C$	$\delta^{18}O_e$	$\delta^{18}O_a$	$\Delta_A{}^{18}O$	Δ_{47e}	Δ_{47a}	$\Delta_A\Delta_{47}$
H. annuus	200	(1)	I	− 2.50 ± 0.02	0.99 ± 0.06	22.5 ± 0.3	25.3 ± 0.1	36.2 ± 0.3	71 ± 2	0.24 ± 0.02	0.54 ± 0.05	1.9 ± 0.3
		(2)	I	− 2.50 ± 0.02	1.20 ± 0.06	22.5 ± 2.3	25.3 ± 0.1	39.2 ± 0.3	77 ± 2	0.24 ± 0.02	0.61 ± 0.05	2.0 ± 0.3
		(3)	I	− 2.50 ± 0.02	1.73 ± 0.06	23.5 ± 0.3	25.3 ± 0.1	40.0 ± 0.3	84 ± 2	0.24 ± 0.02	0.68 ± 0.05	2.4 ± 0.3
	Mean ± SD			**− 2.50**	**1.31 ± 0.38**	**22.8 ± 0.6**	**25.3**	**38.5 ± 2**	**77.3 ± 7**	**0.24**	**0.61 ± 0.07**	**2.10 ± 0.26**
	700	(4)	I	− 2.50 ± 0.02	1.78 ± 0.06	21.6 ± 0.3	25.3 ± 0.1	36.3 ± 0.3	56 ± 2	0.24 ± 0.02	0.48 ± 0.05	1.2 ± 0.3
		(5)	I	− 2.50 ± 0.02	1.22 ± 0.06	20.5 ± 0.3	25.3 ± 0.1	34.8 ± 0.3	52 ± 2	0.24 ± 0.02	0.58 ± 0.05	1.9 ± 0.3
		(6)	I	− 2.50 ± 0.02	1.51 ± 0.06	21.3 ± 0.3	25.3 ± 0.1	35.8 ± 0.3	56 ± 2	0.24 ± 0.02	0.57 ± 0.05	1.7 ± 0.3
		(7)	I	− 2.50 ± 0.02	1.65 ± 0.06	22.5 ± 0.3	25.3 ± 0.1	36.8 ± 0.3	63 ± 2	0.24 ± 0.02	0.61 ± 0.05	2.0 ± 0.3
	Mean ± SD			**− 2.50**	**1.54 ± 0.24**	**21.5 ± 0.8**	**25.3**	**35.9 ± 0.9**	**56.8 ± 5**	**0.24**	**0.56 ± 0.06**	**1.7 ± 0.36**
				− 2.50	1.54 ± 0.24	21.5 ± 0.8	25.3	35.9 ± 0.9	56.8 ± 5	0.24	0.56 ± 0.06	1.70 ± 0.36
	1800	(8)	I	− 2.50 ± 0.02	1.34 ± 0.06	19.8 ± 0.3	25.3 ± 0.1	35.6 ± 0.3	53 ± 2	0.24 ± 0.02	0.45 ± 0.05	1.1 ± 0.3
		(9)	I	− 2.50 ± 0.02	1.18 ± 0.06	20.4 ± 0.3	25.3 ± 0.1	34.6 ± 0.3	53 ± 2	0.24 ± 0.02	0.50 ± 0.05	1.3 ± 0.3
		(10)	I	− 2.50 ± 0.02	1.52 ± 0.06	21.3 ± 0.3	25.3 ± 0.1	35.8 ± 0.3	56 ± 2	0.24 ± 0.02	0.55 ± 0.05	1.6 ± 0.3
	Mean ± SD			**− 2.50**	**1.35 ± 0.17**	**20.5 ± 0.8**	**25.3**	**35.3 ± 0.6**	**54 ± 2**	**0.24**	**0.50 ± 0.05**	**1.33 ± 0.25**
H.hibernica	700	(1)	I	− 2.50 ± 0.02	− 0.53 ± 0.06	10.5 ± 0.3	25.3 ± 0.1	28.8 ± 0.3	18 ± 2	0.24 ± 0.02	0.25 ± 0.05	0.0 ± 0.3
		(2)	I	− 2.50 ± 0.02	− 0.64 ± 0.06	9.4 ± 0.3	25.3 ± 0.1	28.4 ± 0.3	15 ± 2	0.24 ± 0.02	0.29 ± 0.05	0.3 ± 0.3
		(3)	I	− 2.50 ± 0.02	− 0.35 ± 0.06	10.5 ± 0.3	25.3 ± 0.1	29.2 ± 0.3	19 ± 2	0.24 ± 0.02	0.12 ± 0.05	− 0.5 ± 0.3
	Mean ± SD				**− 0.51 ± 0.15**	**10.13 ± 0.6**	**25.3**	**28.80 ± 0.4**	**17.33 ± 2**	**0.24**	**0.22 ± 0.09**	**− 0.07 ± 0.4**
Z. mays	700	(1)	II	− 2.43 ± 0.03	− 1.75 ± 0.06	3.5 ± 0.3	25.5 ± 0.2	28.4 ± 0.3	15 ± 2	0.07 ± 0.03	0.07 ± 0.05	0.0 ± 0.3
		(2)	II	− 2.43 ± 0.03	− 1.75 ± 0.06	3.9 ± 0.3	25.5 ± 0.2	28.3 ± 0.3	16 ± 2	0.07 ± 0.03	0.05 ± 0.05	− 0.1 ± 0.3
		(3)	II	− 2.43 ± 0.03	− 1.78 ± 0.06	3.3 ± 0.3	25.5 ± 0.2	31.6 ± 0.3	31 ± 2	0.07 ± 0.03	0.05 ± 0.05	− 0.1 ± 0.3
	Mean ± SD			**− 2.43**	**− 1.76 ± 0.02**	**3.57 ± 0.31**	**25.5**	**29.43 ± 1.9**	**20.67 ± 9**	**0.07**	**0.06 ± 0.01**	**− 0.07 ± 0.06**

Table 2. Isotopic composition of the CO_2 entering and leaving the leaf cuvette and the resulting isotopic discrimination against the isotopologues $^{13}C^{16}O^{16}O$, $^{12}C^{18}O^{16}O$ and $^{13}C^{18}O^{16}O$ given as $\Delta_A{}^{13}C$, $\Delta_A{}^{18}O$ and $\Delta_A\Delta_{47}$. All the isotope and discrimination values are reported in per mill (‰), with respect to VPDB (for $\delta^{13}C$) and VSMOW (for $\delta^{18}O$). The values in bold are mean and standard deviation for the replicates at different light conditions.

to 60 °C and the evaporated water was directly frozen in a vial cooled to liquid nitrogen temperature[13]. The distillation process was carried out for at least 4 h to ensure quantitative extraction (West et al., 2006). The $\delta^{18}O$ value of the leaf water was determined by equilibrating CO_2 and water in a GasBench II (Thermo Scientific), and subsequent analysis of the oxygen isotope composition of the equilibrated CO_2 with a Delta V mass spectrometer (Thermo Scientific, Germany). The oxygen isotope composition was calibrated versus VSMOW and SLAP.

Results

Gas exchange data and isotopic composition of leaf water.
Gas exchange of *Helianthus* was characterized by high stomatal conductance relative to the other two species (Table 1). The net assimilation A_n was 12 µmol m^{-2} s^{-1} at a PPFD of 200 µmol m^{-2} s^{-1} and increased to 22 µmol m^{-2} s^{-1} at 700 µmol m^{-2} s^{-1}. The net assimilation increased only little further when measured at a PPFD of 1800 µmol m^{-2} s^{-1} (25 µmol m^{-2} s^{-1}). c_i/c_a decreased with increasing irradiance, from 0.82 (at PPFD of 200 µmol m^{-2} s^{-1}) to 0.75 (at 1800 µmol m^{-2} s^{-1}).

Hedera was measured at a PPFD of 700 µmol m^{-2} s^{-1} only where A_n was lower than that of the other two species (15 µmol m^{-2} s^{-1}). Compared to *Helianthus* at the same PPFD, the stomatal conductance g_s was much lower (0.08 mol m^{-2} s^{-1}), causing a clearly lower c_i/c_a ratio (0.41) (Table 1). The C$_4$ species *Zea* was also measured at 700 µmol m^{-2} s^{-1} only where A_n was the highest of the three (28 µmol m^{-2} s^{-1}) but g_s was rather low (0.13 mol m^{-2} s^{-1}) causing the lowest c_i/c_a ratio of the three species, (0.32) (Table 1).

For *Helianthus*, mesophyll conductance calculated using $\Delta_A{}^{13}C$ (g_{m13}) increased with light intensity whereas the mesophyll conductance measured using $\Delta_A{}^{18}O$ (g_{m18}) did not show a clear correlation with the light intensity (Table 1 and Figure S2). Our estimates of g_{m18} had relatively larger errors compared to g_{m13} (Table 1) and the values were larger (Table 1). For *Helianthus*, the g_{m18} estimates were 1.3 to 2.5 times larger and for *Hedera* 1.5 times.

The $\delta^{18}O$ value of the bulk leaf water of *Helianthus* varied between 4.3 and 6.9 ‰ with an average value of 6 ± 1 ‰. For *Hedera*, the bulk leaf water isotopic composition was $\delta^{18}O = 3.1 ± 1.6$ ‰. The relative difference in the $\delta^{18}O$ value of the bulk leaf water between the *Helianthus* and *Hedera* is due to the difference in the $\delta^{18}O$ of source water. For *Zea*, the bulk leaf water isotopic composition of the leaf part inserted in the cuvette was $\delta^{18}O = 20.5 ± 1.3$ ‰. We used a section of the *Zea* leaves at about 1/3 from the tip for gas exchange experiments and such high enrichments in $\delta^{18}O$ of leaf water compared to the source water are typical for sections towards the tip of elongated leaves (see, [65]) and at higher vapor pressure deficit[66].

Effect of photosynthetic gas exchange on the isotopic composition of CO_2.
For *Helianthus* Δ_{47} increased from 0.24 ‰ in the incoming air to 0.50 ‰ to 0.61 ‰ in the outgoing air, at a c_m/c_a ratio of 0.66 to
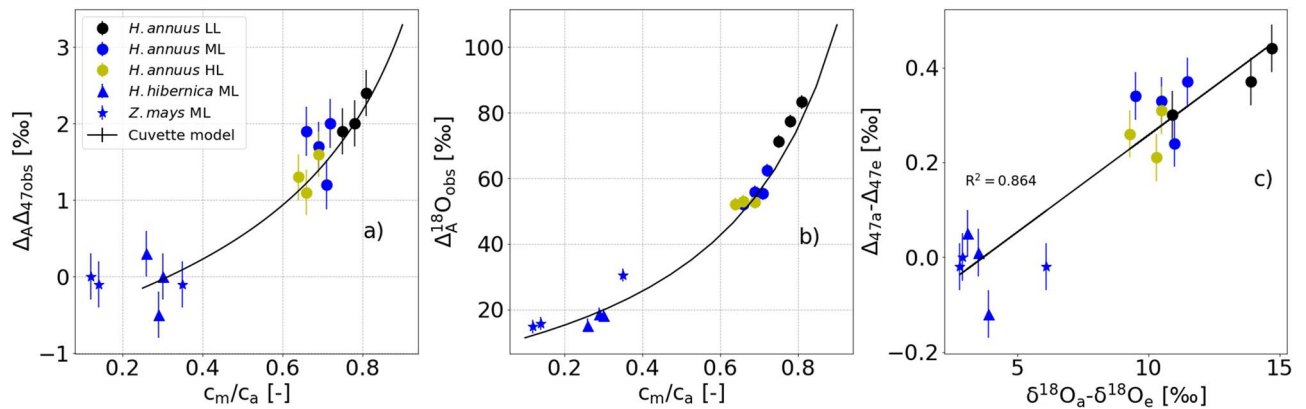
Figure 6. Effect of photosynthetic gas exchange on Δ_{47} and $\delta^{18}O$ of CO_2. $\Delta_A\Delta_{47}$ (**a**) and $\Delta_A^{18}O$ (**b**) during photosynthetic gas exchange experiments as a function of the c_m/c_a ratio. (LL = low light: PPFD = 200 μmol m^{-2} s^{-1}, ML = medium light: PPFD = 700 μmol m^{-2} s^{-1}, HL = high light: PPFD = 1800 μmol m^{-2} s^{-1}). a) discrimination against $^{13}C^{18}O^{16}O$ ($\Delta_A\Delta_{47}$). (**b**) discrimination against $^{12}C^{18}O^{16}O$ ($\Delta_A^{18}O$). (**c**) Relative difference between Δ_{47} the CO_2 entering and leaving the cuvette as a function of the difference between $\delta^{18}O$ of CO_2 entering and leaving the cuvette. The solid line is a linear regression fit with a function of $(\Delta_{47a} - \Delta_{47a}) = (0.041 \pm 0.004) \times (\delta^{18}Oa - \delta^{18}Oe) - 0.151 \pm 0.040$. For the leaf cuvette model, we assumed $\delta^{18}O = 10$ ‰ for the leaf water and a mesophyll conductance of 0.5 mol m^{-2} s^{-1} bar^{-1}.

0.78 (Table 1 and 2). For *Hedera*, at a c_m/c_a ratio of 0.28, the change in Δ_{47} between incoming and outgoing air was more variable than for the other species at similar light intensity. The average change of all the experiments under similar conditions is insignificant (from 0.24 ‰ to 0.22 ‰). For *Zea*, at lower c_m/c_a ratio (0.20), results were more consistent and no statistically significant decrease in Δ_{47} between incoming and outgoing air was observed (Table 1 and 2).

When these changes are converted to discrimination ($\Delta_A\Delta_{47}$), for *Helianthus*, we observed an average $\Delta_A\Delta_{47}$ of 1.7 ± 0.4 ‰. Slightly negative but non-significant discriminations were observed for *Hedera* (-0.07 ± 0.4 ‰), and *Zea* (-0.07 ± 0.06 ‰) (Fig. 6a, Table 2). The $\Delta_A\Delta_{47}$ correlates strongly with the c_m/c_a ratio, higher $\Delta_A\Delta_{47}$ are observed at higher c_m/c_a ratio. The change in Δ_{47} between CO_2 entering and leaving the cuvette correlates strongly with the change in $\delta^{18}O$ of CO_2 entering and leaving the cuvette, with an R^2 value of 0.864 (Fig. 6c). The positive correlation between Δ_{47} and $\delta^{18}O$ of CO_2 indicates that photosynthetic gas exchange affects Δ_{47} and $\delta^{18}O$ similarly (Fig. 6a).

In addition to the $\Delta_A\Delta_{47}$, we also measured $\Delta_A^{13}C$ and $\Delta_A^{18}O$ (Table 2). The average net carbon isotope discrimination was $\Delta_A^{13}C = 21.6 \pm 1.2$ ‰ for *Helianthus*, 10.1 ± 0.7 ‰ for *Hedera* and 3.6 ± 0.3 ‰ for *Zea*. The magnitude of $\Delta_A^{13}C$ also correlates with the c_c/c_a ratio, in agreement with previous studies[13,42,48]. As c_c/c_a depends on light intensity, the gas exchange experiments with *Helianthus* show a slightly higher $\Delta_A^{13}C$ at low light intensity (22.8 ± 0.6 ‰) compared to mid and high light conditions (21.1 ± 0.9 ‰). The average apparent oxygen isotope discrimination $\Delta_A^{18}O$ was 62 ± 12 ‰ for *Helianthus*, 18 ± 3 ‰ for *Hedera* and 21 ± 9 ‰ for *Zea*. Similar to $\Delta_A^{13}C$, $\Delta_A^{18}O$ is higher at low light intensities (78 ± 6 ‰) compared to mid and high light conditions (55 ± 4 ‰) (Table 2, Fig. 6b).

Discussion

The Δ_{47} value of CO_2 has been suggested as a possible tracer for gross primary production, however two previous studies presented contradicting conclusions on the effect of photosynthesis on the Δ_{47} value of CO_2[19,22]. In this study, using a leaf cuvette experiment under controlled conditions (light, CO_2, temperature and humidity) and a leaf cuvette model, we showed that photosynthetic gas exchange can in principle increase or decrease the Δ_{47} value of CO_2 depending on the Δ_{47} value of the CO_2 entering the leaf, the CO_2–H_2O exchange temperature and the back-diffusion flux (quantified as c_m/c_a ratio). However, under conditions similar for the current atmosphere, photosynthesis depletes the Δ_{47} value of atmospheric CO_2.

The photosynthetic effect on Δ_{47} of the residual CO_2 for the C_3 species *Helianthus* and *Hedera* correlated with the CO_2 concentration gradient over the leaf, *i.e.* c_m/c_a, and the discrimination in Δ_{47} showed a similar pattern to $\Delta_A^{18}O$ (Fig. 6). The main driver for the discrimination against $\delta^{18}O$ and Δ_{47} values of CO_2 is isotope exchange with leaf water, and the fractionation associated with the initial fixation by the enzyme RuBisCO (Ribulose-1,5-bisphosphate carboxylase-oxygenase) or PEP (Phosphoenolpyruvate) has no/negligible effect on the $\delta^{18}O$ and Δ_{47} value of CO_2. Δ_{47} value is independent of fractionations in the bulk isotope composition (i.e., variations in $\delta^{18}O$ value due to isotope exchange with leaf water and changes in $\delta^{13}C$ due to metabolic carbon fixation). The lower discrimination in Δ_{47} by C_4 plant *Zea* is due to the lower back-diffusion flux (lower conductance and higher assimilation rate) and the fractionation is dominated by diffusion in agreement with the hypothesis of Eiler and Schauble[19]. Gas phase diffusion causes a decrease in Δ_{47} of the residual CO_2[19], see also Fig. 7.

For *Helianthus*, at a c_m/c_a ratio of 0.81, we observed an increase in Δ_{47} from 0.24 ‰ to 0.68 ‰ (an increase by 0.44 ‰) for a CO_2 drawdown of 100 μmol mol^{-1}. Eiler and Schauble[19] reported an increase in Δ_{47} from 0.65 to 0.75 (an increase by 0.1 ‰, i.e. $\Delta_A \Delta_{47} \sim 0.54$ ‰) due to photosynthetic gas exchange for a CO_2 drawdown of
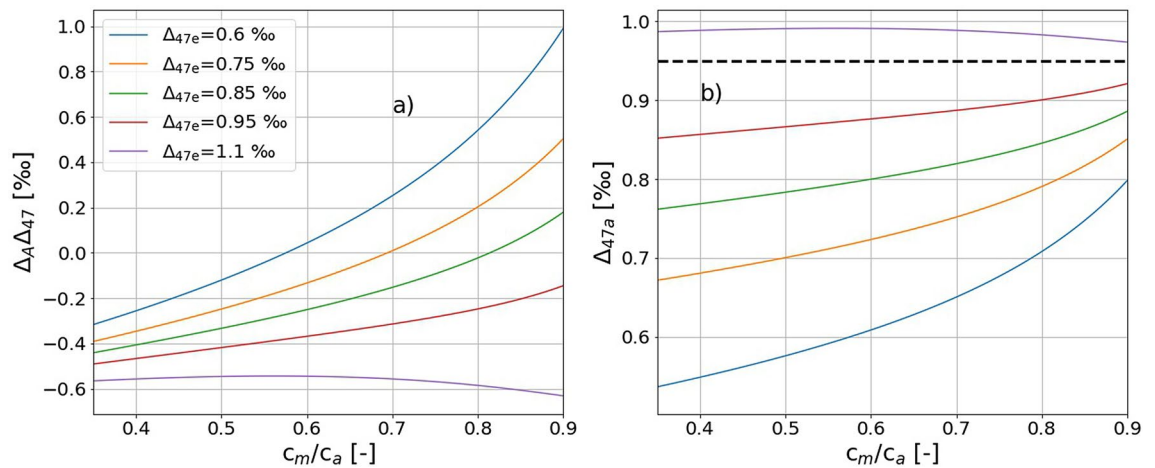
Figure 7. Leaf cuvette model result for Δ_{47} photosynthetic discrimination. (**a**) $\Delta_A\Delta_{47}$ as a function of c_m/c_a for various value of Δ_{47e} (see legend). Panel (**b**) shows the corresponding value for Δ_{47a}, the black dashed line indicates the Δ_{47} of CO_2 at the CO_2-H_2O exchange site for the leaf temperature of 20 °C.

72 μmol mol^{-1} (from 390 to 318) using *Antirrhinum majus* with a c_m/c_a ratio of 0.85, which is consistent with our results.

Using the leaf cuvette model, we quantitatively estimated the expected Δ_{47} discrimination based on the equations discussed in Sect. "Photosynthetic Δ_{47} discrimination" and the derived concentration gradient between the atmosphere and the site of CO_2–H_2O exchange (c_m/c_a). For the C_3 species, we obtained an excellent agreement between the observed and the predicted change in Δ_{47}, except for one outlier for the experiments with *Hedera* (Fig. 6 and Figure S5). For *Zea*, the observed change between outgoing and ingoing CO_2 of − 0.01 ± 0.01 ‰ (the error is standard deviation for the three measurements) was slightly lower than the expected change in Δ_{47} of about + 0.01 ‰. However, the difference was still of the order of our measurement precession.

The correlation between $\Delta_A\Delta_{47}$ and the c_m/c_a ratio and the overall good agreement between observed and predicted $\Delta_A\Delta_{47}$ confirm the hypothesis of Eiler and Schauble[19] that CO_2–H_2O exchange and kinetic fractionation control the discrimination. For high CO_2 back-diffusion fluxes, *i.e.,* high c_m/c_a ratios, the magnitude of the in- and outgoing CO_2 flux is almost the same so that the kinetic term due to diffusion cancels out and the Δ_{47} value of the residual CO_2 is close to the thermodynamic equilibrium value for the respective leaf temperature, *i.e.* $\Delta_{47} = 0.95$ ‰ at 20 °C (Fig. 2). At room temperature, the sensitivity of Δ_{47} to temperature is about 0.005 ‰/°C so that small variations in temperature do not have a large effect. For c_m/c_a ratios close to zero, the back-diffusion flux is small and the kinetic fractionation term due to diffusion into the intercellular airspace induces a negative discrimination in Δ_{47} of up to − 0.08 ‰ if the ingoing CO_2 has a Δ_{47} close to 0 ‰.

As mentioned above and illustrated in Fig. 3, we used CO_2 with an artificially diminished Δ_{47} value in the gas exchange experiments in order to increase the signal, i.e., the Δ_{47} difference between incoming and outgoing CO_2. After having verified the Eiler and Schauble[19] mechanism, we use our leaf cuvette model to quantify the effect of photosynthesis on $\Delta_A\Delta_{47}$ for CO_2 with typical ambient Δ_{47} values. In ambient air, Δ_{47} of CO_2 is usually close to or lower than the Δ_{47} value of CO_2 at the CO_2–H_2O exchange site ($\Delta_{47} = 0.95$ ‰).

Figure 7 illustrates the calculated dependence of $\Delta_A\Delta_{47}$, as well as Δ_{47a} on c_m/c_a during gas exchange for Δ_{47e} values between 0.6 ‰ and 1.1 ‰ to get Δ_{47a} values between 0.6 ‰ and 1.05 ‰ close to the Δ_{47} values of atmospheric CO_2 reported in literature[19–22]. A negative $\Delta_A\Delta_{47}$ means that $_{47a} <_{47e}$ (Eq. 9), i.e., photosynthetic gas exchange would decrease ambient Δ_{47} values, whereas a positive $\Delta_A\Delta_{47}$ would increase ambient Δ_{47} values. Figure 7a shows that $\Delta_A\Delta_{47}$ is mostly negative, thus photosynthetic gas exchange generally acts to decrease Δ_{47} except for situations in which ambient Δ_{47} is at the low end of reported values and c_m/c_a ratios are very high (indicating very slow assimilation rates).

At very low c_m/c_a ratio, i.e., the diffusion limited case, $\Delta_A\Delta_{47}$ is controlled by the diffusional fractionation. Figure 7a shows that $\Delta_A\Delta_{47}$ converges to − 0.5 ‰ as c_m/c_a approaches 0, independent of the incoming CO_2. As indicated in Fig. 2, the theoretically calculated Δ_{47} fractionation associated with diffusion is $\Delta_{47a} - \Delta_{47e} = -0.3$ ‰ when all CO_2 that enters the stomata is assimilated. In our leaf cuvette model where we assume a CO_2 drawdown from 500 to 400 ppm ($\zeta = 500 / (500-400) = 5$), this translates to $\Delta_A\Delta_{47} \approx \zeta \times (\Delta_{47a} - \Delta_{47e}) = -1.5$ ‰). The fact that the model assumes that 2/3 of the CO_2 leave the stomata again without exchanging isotopes explains quantitatively why the diffusion limited endmember is $\zeta \times (\Delta_{47a} - \Delta_{47e})/3 = -0.5$ ‰, independent of the Δ_{47} of CO_2 entering the cuvette. Figure 7a shows that in this limit the value of Δ_{47a} depends very strongly on Δ_{47e}.

For the other extreme scenario $c_m/c_a \approx 1$, Δ_{47a} converges to the Δ_{47} value of CO_2 at the CO_2–H_2O exchange site ($\Delta_{47} = 0.95$ ‰), independent of the Δ_{47} value of incoming CO_2. This reflects the exchange dominated case in Fig. 2. In this case, $\Delta_A\Delta_{47}$ strongly depends on Δ_{47e} value of the CO_2, for instance $\Delta_A\Delta_{47}$ will be ≈ 0.00 ‰ and ≈ − 0.75 ‰ for Δ_{47e} of 0.95 ‰ and 1.1 ‰, respectively. This is similar to what Adnew et al.[13] showed for the ^{17}O-excess of CO_2 in gas exchange experiments.

The leaf cuvette model calculations show that in principle photosynthetic gas exchange can deplete or enrich the Δ_{47} depending on the initial Δ_{47} value of the CO_2 in the air surrounding the leaf, leaf temperature (via the Δ_{47}

value at the exchange site) and the fraction of CO_2 exchanged and diffused back to the atmosphere. However, photosynthesis will enrich Δ_{47} only if the Δ_{47} value of the CO_2 entering the leaf is far lower than the Δ_{47} value of the CO_2 at the CO_2–H_2O exchange site. In addition, Fig. 7b shows that when Δ_{47e} is lower than the equilibrium value of 0.95 ‰, photosynthetic gas exchange cannot lead to Δ_{47a} values above the equilibrium value. Thus, according to our leaf cuvette model, photosynthesis cannot lead to Δ_{47} values that are higher than the thermodynamic equilibrium (unless the incoming, i.e. ambient Δ_{47} values are already higher, in which case they would be reduced). This agrees well with most reported Δ_{47} values of atmospheric CO_2 which are lower than expected from the CO_2–H_2O equilibrium at the surface temperature[19–21].

As a result, an enrichment of up to 0.08 ‰ in Δ_{47} relative to the thermodynamic equilibrium value reported by Laskar and Liang[22] for Δ_{47} measurements of CO_2 sampled in a greenhouse cannot be explained by photosynthesis based on our leaf cuvette model results, even at the extreme scenario of $c_m/c_a \sim 1$. In addition, our results show that photosynthetic driven CO_2–H_2O isotope exchange affects Δ_{47} and $\delta^{18}O$ in a similar way (Fig. 6, Figure S3 and S4) as observed for a simple CO_2–H_2O equilibration experiment[32,33]. This does not support the greenhouse experiment results of Laskar and Liang[22] where they concluded that photosynthesis decouples $\delta^{18}O$ and Δ_{47}. We suggest that other processes than photosynthetic gas exchange affected the greenhouse gas experiments reported earlier[22]. Further experiments in similar environments should be carried out to investigate this in more detail.

Our results provide the experimental verification of the isotope exchange model suggested by Eiler and Schauble[19]. In particular, we determine how $\Delta_A\Delta_{47}$ varies as a function of c_m/c_a. At high c_m/c_a ratio (high back-diffusion flux), the effect of fractionation due to diffusion is negligible and the Δ_{47} of atmospheric CO_2 will be driven towards the Δ_{47} of CO_2 at the CO_2–H_2O exchange site. At low c_m/c_a ratio, the diffusion fractionation dominates and photosynthetic gas exchange will generally lower Δ_{47}. For the real atmosphere with Δ_{47} values slightly lower than the thermodynamic equilibrium set by CO_2–H_2O exchange, photosynthetic gas exchange cannot increase Δ_{47} above this equilibrium value.

Our results also show that Δ_{47} and ^{18}O discrimination are affected in similar ways during photosynthesis, but in contrast to ^{18}O, the clumped isotope composition is independent of the $\delta^{18}O$ of bulk leaf water. This means that it is not necessary to know the precise isotopic composition of water at the CO_2–H_2O exchange site for calculating $\Delta_A\Delta_{47}$. Furthermore, a disequilibrium in Δ_{47} is often identified more readily than in $\delta^{18}O$, since Δ_{47} depends mainly on CO_2–H_2O exchange temperature. As a result, measurements of Δ_{47} during air-leaf gas exchange experiments may be an alternative method to determine the mesophyll conductance to the site of CO_2–H_2O exchange and/or the degree of equilibration between CO_2–H_2O inside the leaf. The limitation to this approach is that the Δ_{47} signals are very small and it requires high precision measurements to constrain the relevant parameters significantly under ambient conditions.

For *Helianthus*, we found g_{m13} values of 0.27 ± 0.1 mol m^{-2} s^{-1} bar^{-1} at a PPFD of 200 μmol m^{-2} s^{-1}, 0.54 ± 0.1 mol m^{-2} s^{-1} bar^{-1} at a PPFD of 700 μmol m^{-2} s^{-1} and 0.43 ± 0.05 mol m^{-2} s^{-1} bar^{-1} at a PPFD of 1800 μmol m^{-2} s^{-1}, in good agreement with values reported in previous studies[41,43,67,68]. These observations confirm earlier findings that the mesophyll conductance is generally lower at low light intensities (Flexas et al., 2007), although we did not observe any significant difference between mid and high light conditions. For *Hedera*, we found a g_{m13} value of 0.20 ± 0.02 mol m^{-2} s^{-1} bar^{-1} at a PPFD of 700 μmol m^{-2} s^{-1}, which is in good agreement with the maximum mesophyll conductance of 0.14 ± 0.01 mol m^{-2} s^{-1} bar^{-1} for evergreen angiosperms, including observations from the *Hedera* species[41,43,51,69]. The higher mesophyll conductance for *Helianthus* compared to *Hedera* might be due to the high mesophyll porosity and thin cell walls of mesophyll cells which facilitate easier movement of CO_2 within intercellular airspaces and across cell walls as reported for evergreen woody plants[70,71].

Mesophyll conductance (g_{m18}) of *Helianthus* did not show a clear dependency on PPFD (Table 1 and Figure S2) with on average a value of 0.68 mol m^{-2} s^{-1} bar^{-1}, which is in good agreement with the few values reported in the literature[41,72]. For maize, $g_{m18} = 0.57$ mol m^{-2} s^{-1} bar^{-1}, which is within the wide range of 0.169 to 0.9 mol m^{-2} s^{-1} bar^{-1} reported in literature[41,73–75]. For *Helianthus* and *Hedera*, g_{m18} is on average 1.7 times g_{m13} confirming that CO_2–H_2O exchange occurs in the mesophyll cell, i.e., before the carboxylation site, in agreement with previous findings[41,47,49,54].

Data availability
All the data used in this manuscript are presented in the form of Figures and Tables.

References
1. Affek, H. P. & Yakir, D. *The stable isotopic composition of atmospheric CO_2*. 2 edn, 179–212 (Elsevier, 2014).
2. Ciais, P., Tans, P. P., Trolier, M., White, J. W. C., Francey, R. J. A large northern hemisphere terrestrial CO_2 sink indicated by the $^{13}C/^{12}C$ ratio of atmospheric CO_2 *Science* **269**, 4 (1995).
3. Ciais, P. *et al.* A three-dimensional synthesis study of $\delta^{18}O$ in atmospheric CO2: 1 Surface fluxes. *J. Geophys. Res. Atmos.* **102**, 5857–5872. https://doi.org/10.1029/96jd02360 (1997).
4. Cuntz, M., Ciais, P., Hoffmann, G. & Knorr, W. A comprehensive global three-dimensional model of $\delta^{18}O$ in atmospheric CO2: 1. Validation of surface processes. *J. Geophys. Res. Atmos.* **108**, 24 (2003).
5. Cuntz, M. A dent in carbon's gold standard. *Nature* **477**, 547–548 (2011).
6. Welp, L. R. *et al.* Interannual variability in the oxygen isotopes of atmospheric CO_2 driven by El Niño. *Nature* **477**, 579–582. https://doi.org/10.1038/nature10421 (2011).
7. Adnew, G. A. *et al.* Determination of the triple oxygen and carbon isotopic composition of CO_2 from atomic ion fragments formed in the ion source of the 253 Ultra High-Resolution Isotope Ratio Mass Spectrometer. *Rapid Commun. Mass Spectrom.* **33**, 17 (2019).
8. Hoag, K. J., Still, C. J., Fung, I. Y. & Boering, K. A. Triple oxygen isotope composition of tropospheric carbon dioxide as a tracer of terrestrial gross carbon fluxes. *Geophys. Res. Lett.* https://doi.org/10.1029/2004gl021011 (2005).

9. Thiemens, M. K., Chakraborty, S. & Jackson, T. L. Decadal $\Delta^{17}O$ record of tropospheric CO_2: verification of a stratospheric component in the troposphere. *J. Geophys. Res. Atmos.* **119**, 8 (2014).
10. Hofmann, M. E. G. *et al.* Atmospheric measurements of $\Delta^{17}O$ in CO_2 in Göttingen, Germany reveal a seasonal cycle driven by biospheric uptake. *Geochim. Cosmochim. Ac.* **199**, 143–163. https://doi.org/10.1016/j.gca.2016.11.019 (2017).
11. Liang, M.-C., Mahata, S., Laskar, A. H., Thiemens, M. H. & Newman, S. Oxygen isotope anomaly in tropospheric CO_2 and implications for CO_2 residence time in the atmosphere and gross primary productivity. *Sci. Rep.* **7**, 13180. https://doi.org/10.1038/s41598-017-12774-w (2017).
12. Koren, G. *et al.* Global 3-D Simulations of the Triple Oxygen Isotope Signature $\Delta^{17}O$ in Atmospheric CO_2. *J. Geophys. Res. Atmos.* **124**, 28 (2019).
13. Adnew, G. A., Pons, T. L., Koren, G., Peters, W. & Röckmann, T. Leaf-scale quantification of the effect of photosynthetic gas exchange on $\Delta^{17}O$ of atmospheric CO_2. *Biogeosciences* **17**, 3903–3922 (2020).
14. Liang, M.-C. & Mahata, S. Oxygen anomaly in near surface carbon dioxide reveals deep stratospheric intrusion. *Sci. Rep.* **5**, 11352. https://doi.org/10.1038/srep11352 (2015).
15. Mahata, S., Chung-Ho, W., Bhattacharya, S. K. & Mao-Chang, L. Near Surface CO_2 triple oxygen isotope composition. *Terrest. Atmos. Ocean. Sci.* **27**, 7 (2016).
16. Laskar, A. M., Mahata, S., Bhattacharya, S. K. & Liang, M.-C. Triple oxygen and clumped isotope compositions of CO2 in the middle troposphere. *Earth Space Sci.* **6**, 1205–1219 (2019).
17. Levin, I. a. K., Bernd and Schmidt, Martina and Sartorius, Hartmut. A novel approach for independent budgeting of fossil fuel CO_2 over Europe by $^{14}CO_2$ observations. *Geophys. Res. Lett.*, 2194 (2003).
18. Turnbull, J. C. *et al.* Assessment of fossil fuel carbon dioxide and other anthropogenic trace gas emissions from airborne measurements over Sacramento, California in spring 2009. *Atmos. Chem. Phys.* **11**, 705–721 (2011).
19. Eiler, J. M. & Schauble, E. $^{18}O^{13}C^{16}O$ in Earth's atmosphere. *Geochim. Cosmochim. Acta* **68**, 10 (2004).
20. Affek, H. P. & Eiler, J. M. Abundance of mass 47 CO_2 in urban air, car exhaust, and human breath. *Geochim. Cosmochim. Acta.* **70**, 12. https://doi.org/10.1016/j.gca.2005.08.021 (2006).
21. Affek, H. P., Xu, X. & Eiler, J. M. Seasonal and diurnal variations of $^{13}C^{18}O^{16}O$ in air: Initial observations from Pasadena CA. *Geochim. Cosmochim. Acta* **71**, 5033–5043. https://doi.org/10.1016/j.gca.2007.08.014 (2007).
22. Laskar, A. H. & Liang, M.-C. Clumped isotopes in near-surface atmospheric CO_2 over land, coast and ocean in Taiwan and its vicinity. *Biogeosciences* **13**, 7 (2016).
23. Röckmann, T., Popa, M. E., Krol, M. C. & Hofmann, M. E. G. Statistical clumped isotope signatures. *Sci. Rep.* **6**, 31947 (2016).
24. Wang, Z., Schauble, E. A. & Eiler, J. M. Equilibrium thermodynamics of multiply substituted isotopologues of molecular gases. *Geochim. Cosmochim. Acta.* **68**, 4779–4797 (2004).
25. Dennis, K. J., Affek, H. P., Passey, B. H., Schrag, D. P. & Eiler, J. M. Defining an absolute reference frame for 'clumped' isotope studies of CO_2. *Geochim. Cosmochim. Acta* **75**, 7117–7131 (2011).
26. Affek, H. P., Xu, X. & Eiler, J. M. Seasonal and diurnal variations of 13C18O16O in air: Initial observations from Pasadena CA. *Geochim. Cosmochim. Acta* **71**, 10 (2007).
27. Francey, R. J. & Tans, P. P. Latitudinal variation in oxygen-18 of atmospheric CO_2. *Nature* **327**, 2 (1987).
28. Farquhar, G. D. *et al.* Vegetation effects on the isotope composition of oxygen in atmospheric CO2. *Nature* **363**, 439–443 (1993).
29. Gillon, J. S. & Yakir, D. Influence of carbonic anhydrase activity in terrestrial vegetation on the ^{18}O content of atmospheric CO_2 *Science* **291**, 3 (2001).
30. Wingate, L. *et al.* The impact of soil microorganisms on the global budget of $\delta^{18}O$ in atmospheric CO_2. *PNAS* **106**, 4 (2009).
31. Ogée, J., Wingate, L. & Genty, B. Estimating mesophyll conductance from measurements of $C^{18}OO$ photosynthetic discrimination and carbonic anhydrase activity. *Plant Physiol.* **178**, 728–752 (2018).
32. Affek, H. P. Clumped isotopic equilibrium and the rate of isotope exchange between CO_2 and water. *Am J. Sci.* **313**, 16. https://doi.org/10.2475/04.2013.02 (2013).
33. Clog, M., Stolper, D. & Eiler, J. M. Kinetics of CO_2 $_{(g)}$–H_2O $_{(l)}$ isotopic exchange, including mass 47 isotopologues. *Chem. Geol.* **395**, 10 (2015).
34. Dai, A. Recent climatology, variability, and trends in global surface humidity. *J. Clim.* **19**, 17 (2006).
35. Daëron, M., Blamart, D., Peral, M. & Affek, H. P. Absolute isotopic abundance ratios and the accuracy of Δ_{47} measurements. *Chem. Geol.* **442**, 13. https://doi.org/10.1016/j.chemgeo.2016.08.014 (2016).
36. Craig, H. Isotopic standards for carbon and oxygen and correction factors for mass-spectrometric analysis of carbon dioxide. *Geochim Cosmochim Ac.* **12**, 16. https://doi.org/10.1016/0016-7037(57)90024-8 (1957).
37. Brand, W. A., Assonov, S. S. & Coplen, T. B. Correction for the ^{17}O interference in $\delta^{13}C$ measurements when analyzing CO_2 with stable isotope mass spectrometry (IUPAC Technical Report). *Pure Appl. Chem.* **82**, 1719–1733. https://doi.org/10.1351/pac-rep-09-01-05 (2010).
38. Schauer, A. J., Kelson, J., Saenger, C. & Huntington, K. W. Choice of ^{17}O correction affects clumped isotope (Δ_{47}) values of CO_2 measured with mass spectrometry. *Rapid Commun. Mass Spectrom.* **30** (2016).
39. Ubierna, N. *et al.* Critical review: incorporating the arrangement of mitochondria and chloroplasts into models of photosynthesis and carbon isotope discrimination. *Photosynth. Res.* **141**, 26 (2019).
40. Cousins, A. B., Mullendore, D. L., Sonawane, B. V. Recent developments in mesophyll conductance in C_3, C_4 and CAM plants *Plant J.* **101**, 816–830 (2020).
41. Adnew, G. A. The effect of photosynthetic gas exchange on $\Delta^{17}O$ of atmospheric CO_2. *PhD thesis.* doi:https://doi.org/10.33540/412 (2020).
42. Farquhar, G. D., Ehleringer, J. R. & Hubick, K. T. Carbon isotope discrimination and photosynthesis. *Annu. Rev. Plant Physiol. Plant Mol. Biol.* **40**, 503–537 (1989).
43. Flexas, J., Ribas-Carbo, M., Diaz-Espejo, A., Galmes, J. & Medrano, H. Mesophyll conductance to CO_2: current knowledge and future prospects. *Plant Cell Environ.* **31**, 19 (2008).
44. Busch, F. A., Holloway-Phillips, M., Stuart-Williams, H. & Farquhar, G. D. Revisiting carbon isotope discrimination in C_3 plants shows respiration rules when photosynthesis is low. *Nat. Plants* **6**, 245–258 (2020).
45. Farquhar, G. D. & Richards, R. A. Isotopic composition of plant carbon correlates with water-use efficiency of wheat genotypes. *Funct. Plant Biol.* **11**, 11 (1984).
46. Farquhar, D. G. & Lloyd, J. *Carbon and oxygen isotope effects in the exchange of carbon dioxide between terrestrial plants and the atmosphere*. 33 (Acadamic Press Inc., 1993).
47. Barbour, M. M., Evans, J. R., Simonin, K. A. & Caemmerer, S. v. Online CO_2 and H_2O oxygen isotope fractionation allows estimation of mesophyll conductance in C_4 plants, and reveals that mesophyll conductance decreases as leaves age in both C_4 and C_3 plants. *New Phytol.*, 875–889 (2016).
48. Evans, J. R., Sharkey, T. D., Berry, J. A. & Farquhar, G. D. Carbon isotope discrimination measured concurrently with gas exchange to investigate CO_2 diffusion in leaves of higher plants. *Funct Plant. Biol.* **13**, 11 (1986).
49. Gillon, J. S. & Yakir, D. Internal conductance to CO_2 diffusion and $C^{18}OO$ discrimination in C_3 leaves. *Plant Physiol.* **123**, 13 (2000).
50. Caemmerer, S. v., Ghannoum, O., Pengelly, J. J. L. & Cousins, A. B. Carbon isotope discrimination as a tool to explore C_4 photosynthesis. *J. Exp. Bot.* **65**, 3459 (2014).

51. Pons, T. L. *et al.* Estimating mesophyll conductance to CO_2: methodology, potential errors, and recommendations. *J. Exp. Bot.* **60**, 7 (2009).
52. Holloway-Phillips, M., Cernusak, L. A., Stuart-Williams, H., Ubierna, N. & Farquhar, G. D. Two-source $\delta^{18}O$ method to validate the $CO^{18}O$-photosynthetic discrimination model: implications for mesophyll conductance. *Plant Physiol.* **181**, 15 (2019).
53. Cernusak, L. A., Farquhar, G. D., Wong, S. C. & Stuart-Williams, H. Measurement and interpretation of the oxygen isotope composition of carbon dioxide respired by leaves in the dark. *Plant Physiol.* **136**, 13 (2004).
54. Gillon, J. S. & Yakir, D. Naturally low carbonic anhydrase activity in C_4 and C_3 plants limits discrimination against $C^{18}OO$ during photosynthesis. *Plant Cell Environ.* **23**, 12 (2000).
55. Song, X., Simonin, K. A., Loucos, K. E. & Barbour, M. M. Modelling non-steady-state isotope enrichment of leaf water in a gas-exchange cuvette environment. *Plant Cell Environ.* **38**, 10 (2015).
56. Parkinson, K. J. A simple method for determining the boundary layer resistance in leaf cuvettes. *Plant Cell Environ* **8**, 223–226 (1985).
57. Laskar, A. H., Mahata, S. & Liang, M.-C. Identification of anthropogenic CO_2 using triple oxygen and clumped isotopes. *Environ. Sci. Technol.* **50**, 18. https://doi.org/10.1021/acs.est.6b02989 (2016).
58. Defliese, W. F. & Lohmann, K. C. Non-linear mixing effects on mass-47 CO_2 clumped isotope thermometry: patterns and implications. *Rapid Commun. Mass Spectrom.* **29**, 901–909 (2017).
59. Gillon, G., Adnew, G. A., Röckmann, T. & Peters, W. Leaf conductance model for ^{17}O in CO_2, https://git.wur.nl/leaf_model. (2020).
60. Pons, T. L. & Welschen, R. A. M. Technical report; Overestimation of respiration rates in commercially available clamp-on leaf chambers. Complications with measurement of net photosynthesis. *Plant, Cell Environ.* **25**, 1367–1372. https://doi.org/10.1093/jxb/erp081 (2002).
61. von Caemmerer, S. & Farquhar, G. D. Some relationships between the biochemistry of photosynthesis and the gas exchange of leaves. *Planta* **153**, 376–387 (1981).
62. Werner, R. A., Rothe, M. & Brand, W. A. Extraction of CO_2 from air samples for isotopic analysis and limits to ultra high precision $\delta^{18}O$ determination in CO_2 gas. *Rapid Commun. Mass Spectrom.* **15**, 2152–2167 (2001).
63. Werner, R. A. & Brand, W. A. Referencing strategies and techniques in stable isotope ratio analysis. *Rapid Commun Mass Spectrom* **15**, 501–519. https://doi.org/10.1002/rcm.258 (2001).
64. Huntington, K. W. *et al.* Methods and limitations of 'clumped' CO_2 isotope (Δ_{47}) analysis by gas-source isotope ratio mass spectrometry. *J. Mass Spectrom.* **44**, 11 (2009).
65. Cernusak, L. A. *et al.* Stable isotopes in leaf water of terrestrial plants. *Plant Cell Environ.* **39**, 1087–1102. https://doi.org/10.1111/pce.12703 (2016).
66. Farquhar, G. D., Cernusak, L. A. & Barnes, B. Heavy water fractionation during transpiration. *Plant Physiol.* **143**, 7 (2007).
67. Hanba, Y. T., Kogami, H. & Terashima, I. The effect of internal CO_2 conductance on leaf carbon isotope ratio. *Isotopes Environ. Health Stud* **39**, 5–13. https://doi.org/10.1080/1025601031000102233 (2003).
68. Laisk, A. & Loreto, F. Determining photosynthetic parameters from leaf CO_2 exchange and chlorophyll fluorescence (ribulose-1, 5-bisphosphate carboxylase/oxygenase specificity factor, dark respiration in the light, excitation distribution between photosystems, alternative electron transport rate, and mesophyll diffusion resistance. *Plant Physiol.* **110**, 9 (1996).
69. Loreto, F., Harley, P. C., Marco, G. D. & Sharkey, T. D. Estimation of mesophyll conductance to CO_2 flux by three different methods. *Plant Physiol.* **98**, 6 (1992).
70. Veromann-Jürgenson, L.-L., Tosens, T., Laanisto, L. & Niinemets, ü. Extremely thick cell walls and low mesophyll conductance: welcome to the world of ancient living!. *Journal of Experimental Botany* **68** (2017).
71. Niinemets, Ü. Does the touch of cold make evergreen leaves tougher?. *Tree Physiol.* **36**, 5 (2016).
72. Shrestha, A., Song, X. & Barbour, M. M. The temperature response of mesophyll conductance, and its component conductances, varies between species and genotypes. *Photosynth. Res.*, 18 (2019).
73. Ubierna, N., Gandin, A., Boyd, R. A. & Cousins, A. B. Temperature response of mesophyll conductance in three C_4 species calculated with two methods: ^{18}O discrimination and in vitro Vpmax. *New Phytol.* **214**, 66–80 (2017).
74. Kolbe, A. R. & Cousins, A. B. Mesophyll conductance in Zea mays responds transiently to CO_2 availability: implications for transpiration efficiency in C_4 crops. *New Phytol.* **217**, 11 (2018).
75. Ubierna, N., Gandin, A. & Cousins, A. B. The response of mesophyll conductance to short-term variation in CO_2 in the C_4 plants Setaria viridis and Zea mays *Journal of experimental botany* **69**, 11 (2018).

Acknowledgements

Author contributions

M.E.G.H. and T.R. designed the experiment, T.P. and M.E.G.H. performed the leaf cuvette experiment and air sampling. G.A.A., T.P., M.E.G.H. and T.R. evaluated the data. G.K. provided the leaf cuvette model calculations. G.A.A., M.E.G.H. and T.R. wrote the manuscript with contributions from T.P., G.K., M.Z., and L.J.L.

Competing interests

The authors declare no competing interests.

Additional information

Supplementary Information The online version contains supplementary material available at https://doi.org/10.1038/s41598-021-93092-0.

Correspondence and requests for materials should be addressed to G.A.A.

Reprints and permissions information is available at www.nature.com/reprints.

Publisher's note Springer Nature remains neutral with regard to jurisdictional claims in published maps and institutional affiliations.